isvr Institute of Sound and Vibration Research

The Influence of the Source and Receiver Modal Behaviour on Power Transmission between Two Subsystems

W.S. Park, D.J. Thompson and N.S. Ferguson

ISVR Technical Memorandum 861

March 2001

University of Southampton

SCIENTIFIC PUBLICATIONS BY THE ISVR

Technical Reports are published to promote timely dissemination of research results by ISVR personnel. This medium permits more detailed presentation than is usually acceptable for scientific journals. Responsibility for both the content and any opinions expressed rests entirely with the author(s).

Technical Memoranda are produced to enable the early or preliminary release of information by ISVR personnel where such release is deemed to the appropriate. Information contained in these memoranda may be incomplete, or form part of a continuing programme; this should be borne in mind when using or quoting from these documents.

Contract Reports are produced to record the results of scientific work carried out for sponsors, under contract. The ISVR treats these reports as confidential to sponsors and does not make them available for general circulation. Individual sponsors may, however, authorize subsequent release of the material.

UNIVERSITY OF SOUTHAMPTON

INSTITUTE OF SOUND AND VIBRATION RESEARCH

DYNAMICS GROUP

The Influence of the Source and Receiver Modal Behaviour on Power Transmission between Two Subsystems

by

W. S. Park, D. J. Thompson and N.S. Ferguson

ISVR Technical Memorandum No. 861

March 2001

Authorized for issue by
Dr. M.J. Brennan
Group Chairman

CONTENTS

1. INTRODUCTION

The use of Statistical Energy Analysis (SEA) to predict the response of vibro-acoustic systems relies on good estimates of the damping loss factors of subsystems and the coupling loss factors (CLFs) between them. Damping is usually estimated from measurement data. The CLFs are therefore normally the main parameters that are difficult to evaluate experimentally or numerically. Usually theoretical estimates of the CLF, based on the wave transmission between infinite subsystems, are used.

For two infinite subsystems coupled along a line or at a surface, the wave transmission efficiency, τ, is defined as the ratio of the transmitted power to the incident power [1]. By integrating over all possible angles of incidence, the diffuse incidence transmission efficiency can be determined.

The CLF estimates determined from these transmission efficiencies, for infinite subsystems, are taken as representative of ensemble averages of finite subsystems. At low modal overlap, usually corresponding to low frequency, the actual energy transfer between subsystems can differ considerably from that predicted using these estimates [2]. These fluctuations are in part due to the particular realisation of the subsystems within the notional ensemble. Underlying the fluctuations are the modal properties of the subsystems. Their damping also plays a role in determining the extent of the fluctuations.

In [2] it was shown that, for two finite rectangular plates coupled along a line, the modal behaviour of the plates affects the coupling, expressed as an 'effective CLF' (to distinguish it from the ensemble average CLF). Craik *et al.* [3] proposed that only the modal properties of the receiving subsystem affect coupling between two subsystems. Using FE predictions, Steel *et al.* [4] verified numerically the earlier experimental work. However, it was not clear in the results in [2] whether it is the modal behaviour of the source or receiver plate or both that is responsible for these fluctuations compared to the results for infinite subsystems. Therefore, in this report, models are considered of a finite source plate coupled to an infinite receiver and vice versa. First, however, a model of two semi-infinite plates of finite width is introduced to investigate the effect of the finite width compared with the results for coupled semi-infinite plates of infinite width.

2. SEMI-INFINITE PLATES OF FINITE WIDTH

Before considering finite plates, the restriction imposed by a finite width is studied. Consider two semi-infinite plates, which are simply supported along the longitudinal edges, $y = 0$ and $y = b$, and joined at the interface $x = 0$, as shown in Figure 2.1. At $x = 0$ a simple support is assumed, which could also represent a right-angled joint in the absence of in-plane motion.

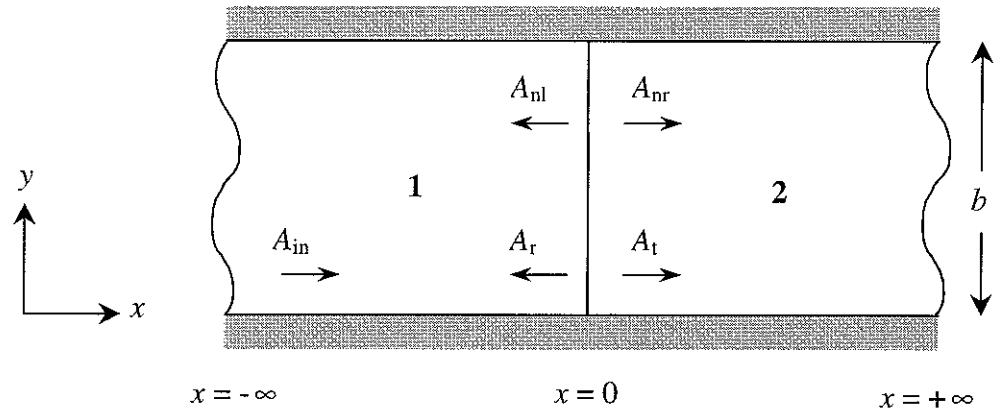

Figure 2.1. Two semi-infinite aluminium plates of finite width b joined at a line.

Allowable wave solutions have a trace wavenumber in the y direction k_n ($=n\pi/b$) for integer values of n. Considering only flexural waves, an exact analytical expression for the motion of plate 1 of order n is

$$w_1(x, y) = (A_{in}e^{-k_1 x} + A_r e^{k_1 x} + A_{nl}e^{k_2 x}) \sin(k_n y) \tag{2.1}$$

where A_{in}, A_r and A_{nl} are the complex amplitudes of the incident, reflected propagating and nearfield waves at the interface, and k_1 and k_2 are the respective propagating and nearfield wavenumbers of plate 1. These wavenumbers are the roots obtained from the wave equation for plate 1, *i.e.*

$$k_1 = (k_n^2 - k_{f1}^2)^{1/2} \tag{2.2}$$

$$k_2 = (k_n^2 + k_{f1}^2)^{1/2} \tag{2.3}$$

where k_{f1} ($=(\rho_1 h_1 \omega^2/D_1)^{1/4}$) is the free bending wavenumber of plate 1.

The effective angle of incidence θ at the interface $x = 0$ can be obtained from

$$\theta = \tan^{-1}\left|\frac{k_n}{k_1}\right| \tag{2.4}$$

where $\theta = 0$ corresponds to normal incidence.

Similarly for plate 2,

$$w_2(x, y) = (A_t e^{-k_3 x} + A_{nr} e^{-k_4 x}) \sin(k_n y) \tag{2.5}$$

where A_t and A_{nr} are the complex amplitudes of the transmitted propagating and nearfield waves at the interface, and k_3 and k_4 are the respective wavenumbers of plate 2. These wavenumbers are the roots obtained from the wave equation for plate 2,

$$k_3 = (k_n^2 - k_{f2}^2)^{1/2} \tag{2.6}$$

$$k_4 = (k_n^2 + k_{f2}^2)^{1/2} \tag{2.7}$$

where k_{f2} $(=(\rho_2 h_2 \omega^2 / D_2)^{1/4})$ is the free bending wavenumber of plate 2.

Constraining the displacement along the joint, only rotational motion is allowed. Applying the equilibrium and continuity conditions at the joint, one can determine the amplitude of each wave: *i.e.*

(1) displacements at the joint

$$w_1(0, y) = 0 \tag{2.8}$$

$$w_2(0, y) = 0 \tag{2.9}$$

(2) rotations at the joint

$$\frac{\partial w_1(0, y)}{\partial x} = \frac{\partial w_2(0, y)}{\partial x} \tag{2.10}$$

(3) bending moments at the joint

$$M_{xx,1}(0, y) = D_1 \left\{ \frac{\partial^2 w_1}{\partial x^2} + \nu_1 \frac{\partial^2 w_1}{\partial y^2} \right\}_{x=0} = M_{xx,2}(0, y) = D_2 \left\{ \frac{\partial^2 w_2}{\partial x^2} + \nu_2 \frac{\partial^2 w_2}{\partial y^2} \right\}_{x=0} \tag{2.11}$$

Substituting equations (2.1) and (2.5) into these boundary conditions (2.8) - (2.11), the four unknown amplitudes can be determined in terms of the amplitude of the incident wave A_{in}, as follows.

$$A_r + A_{nl} + A_{in} = 0 \tag{2.12}$$

$$A_t + A_{nr} = 0 \tag{2.13}$$

$$k_1 A_r + k_2 A_{nl} - k_1 A_{in} = -k_3 A_t - k_4 A_{nr} \tag{2.14}$$

$$\begin{aligned} &D_1\left[(k_1^2 - \nu_1 k_n^2)A_r + (k_2^2 - \nu_1 k_n^2)A_{nl} + (k_1^2 - \nu_1 k_n^2)A_{in}\right] = \\ &D_2\left[(k_3^2 - \nu_2 k_n^2)A_t + (k_4^2 - \nu_2 k_n^2)A_{nr}\right] \end{aligned} \tag{2.15}$$

Equations (2.12) - (2.15) can be written in matrix form,

$$\boldsymbol{B}_1 \boldsymbol{A}_1 = \boldsymbol{C}_1 \tag{2.16}$$

where

$$\boldsymbol{B}_1 = \begin{bmatrix} 1 & 1 & 0 & 0 \\ 0 & 0 & 1 & 1 \\ k_1 & k_2 & k_3 & k_4 \\ D_1(k_1^2 - \nu_1 k_n^2) & D_1(k_2^2 - \nu_1 k_n^2) & -D_2(k_3^2 - \nu_2 k_n^2) & -D_2(k_4^2 - \nu_2 k_n^2) \end{bmatrix} \tag{2.17}$$

$$\boldsymbol{A}_1 = \begin{bmatrix} \frac{A_r}{A_{in}} & \frac{A_{nl}}{A_{in}} & \frac{A_t}{A_{in}} & \frac{A_{nr}}{A_{in}} \end{bmatrix}^T \tag{2.18}$$

and

$$\boldsymbol{C}_1 = \begin{bmatrix} -1 & 0 & k_1 & -D_1(k_1^2 - \nu_1 k_n^2) \end{bmatrix}^T . \tag{2.19}$$

Above cut-on, power is transmitted by the propagating waves, but not by the near-field waves. In general the powers are proportional to the wave amplitude squared, but also depend on the plate properties. The incident and reflected waves exist in the same plate so the transmission efficiency τ can be obtained from

$$\tau = 1 - \left|\frac{A_r}{A_{in}}\right|^2 . \tag{2.20}$$

Figure 2.2 shows example results for a source plate of thickness 3 mm and a receiver plate of thickness 2 mm, both of aluminium with no damping. The transmission efficiency only exists above the cut-on frequency for any particular value of n of plate 1. Below the cut-on frequency in plate 1, no propagating incident wave will occur and it is meaningless to calculate the transmission efficiency. When the cut-on frequency in the source plate is higher than in the receiver plate, no energy will be transmitted into pure propagating waves in the receiver plate below its cut-on frequency and the transmission efficiency is zero. Thus the transmission efficiencies are zero up to the higher of the two cut-on frequencies. Then they rise gradually and tend to the result for normal incidence on semi-infinite plates at high frequencies. This can be explained by consideration of the angle of incidence, equation (2.4). At cut-on, $k_n = k_f$ and wave propagation occurs in a direction parallel to the joint, *i.e.* $k_1 = 0$.

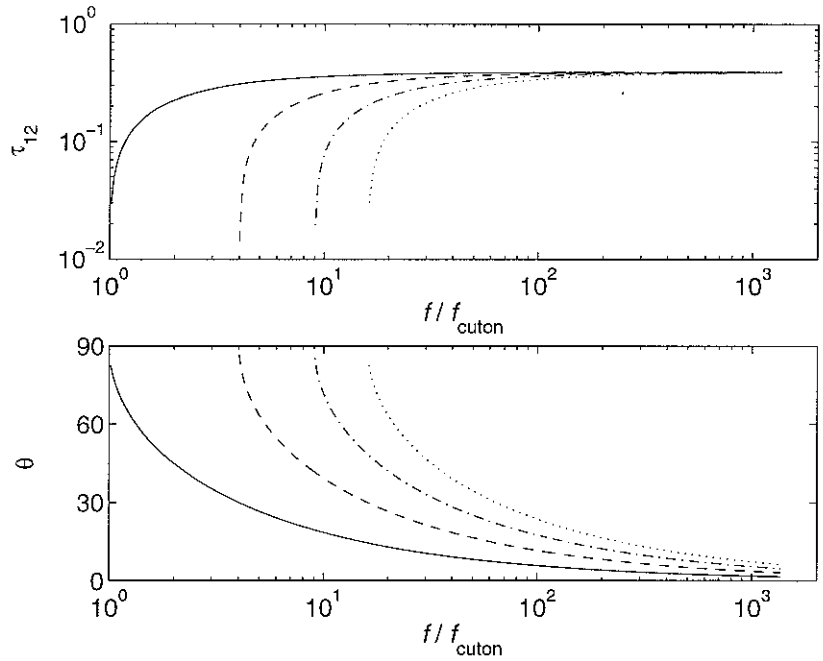

Figure 2.2. Transmission efficiencies and the angle of incidence predicted for two semi-infinite aluminium plates of width $b = 1$m, thickness of the source plate $h_1 = 3$mm, and the thickness of the receiver plate $h_2 = 2$mm. Four curves present the results for different transverse orders, n; —, $n = 1$; ---, $n = 2$; –·–, $n = 3$; ····, $n = 4$. The x-axis is a non-dimensional frequency, f / f_{cuton}, for f_{cuton} of the source plate for $n = 1$ ($f_{\text{cuton}} = 7.34$ Hz).

The transmission efficiency for oblique incidence is given by [1]

$$\tau_{12}(\theta) = \frac{2\psi\sqrt{\chi^2 - s^2}\sqrt{1-s^2}}{\psi^2 + \psi\left(\sqrt{\chi^2 + s^2}\sqrt{1+s^2} + \sqrt{\chi^2 - s^2}\sqrt{1-s^2}\right) + \chi^2} \tag{2.21}$$

where, for plates of identical material $\chi = \sqrt{h_1/h_2}$, $\psi = (h_2/h_1)^2$, $s = \sin\theta$, and θ is the angle of incidence. For such grazing incidence $\theta = \pm\pi/2$, τ_{12} is zero. As the frequency increases, the propagating direction gradually approaches normal incidence $\theta \rightarrow 0$ and τ, for a given n, tends to $\tau_{12}(0)$. As more orders across the plate width, n, cut on and are included in the incident field, this approximates more closely to a diffuse field, with the incident energy not primarily being at a single angle of incidence. Thus the sum of all such n will tend to the diffuse field value of $\tau_{12,d}$ found from infinite plates.

The CLF is only defined for finite plates. The transmission efficiency, τ, for two semi-infinite plates can be used to estimate the CLF of an equivalent finite plate by using the expression [1]

$$\eta_{12\infty} = \frac{c_{g1} b \tau_{12}}{\pi \omega S_1} \tag{2.22}$$

where c_{g1} is the group velocity of subsystem 1, b is the junction length, τ_{12} is the transmission efficiency, and S_1 is the surface area of the source subsystem ($=bL_1$, for a rectangular plate of length L_1). The CLF results, using these semi-infinite plate transmission efficiencies for particular transverse orders, are shown in Figure 2.3 for a source plate of area 0.5 m^2.

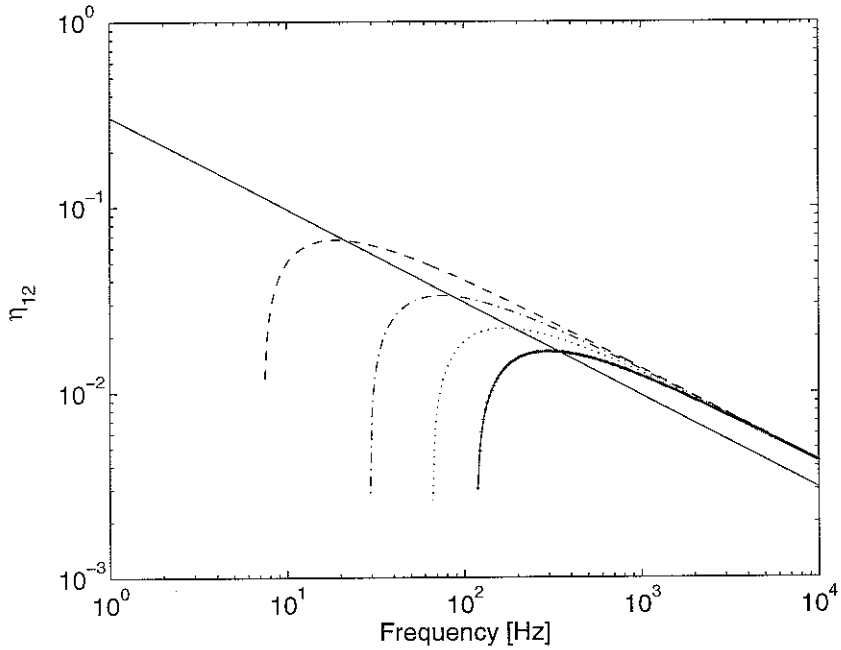

Figure 2.3. Coupling loss factors derived from models of two infinite plates and of two semi-infinite plates of finite width; —, $\eta_{12\infty}$; ---, $n = 1$; -·-, $n = 2$; ···, $n = 3$; -+-, $n = 4$.

3. SEMI-INFINITE SOURCE PLATE OF FINITE WIDTH COUPLED TO A FINITE RECEIVER PLATE

3.1 Model

In this section, a model is considered in which a semi-infinite source plate is connected to a finite receiver plate of length L_2. The right-hand edge of plate 2 is assumed to be free. This model is used to investigate the influence of the modal behaviour of the receiver plate on the energy transmission. An incident wave A_{in} is applied into the semi-infinite source plate as in the previous section. The transmission efficiencies are evaluated for different thickness ratios of the source to receiver plate and the results are considered in terms of the modal behaviour of the finite receiver plate.

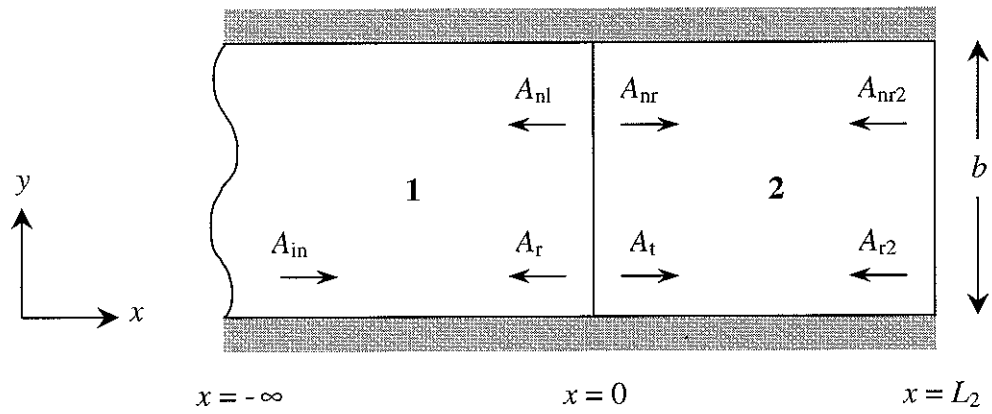

Figure 3.1. Semi-infinite (source) plate of finite width b connected to a finite (receiver) plate.

The out-of-plane displacement of plate 2 given in equation (2.5) must be extended to include a second reflected wave and a second nearfield wave.

$$w_2(x,y) = (A_t e^{-k_3 x} + A_{nr} e^{-k_4 x} + A_{r2} e^{k_3 x} + A_{nr2} e^{k_4 x}) \sin(k_n y) \tag{3.1}$$

where A_{r2} and A_{nr2} are the complex amplitudes of the reflected propagating and nearfield waves at the right-hand edge of plate 2. Applying the equilibrium and continuity conditions at the joint and boundary conditions at the right-hand free edge of plate 2 to this equation and equation (2.1), the six unknown amplitudes can be solved in terms of A_{in}. Equations (2.13)-(2.15) can be modified to

$$A_t + A_{nr} + A_{r2} + A_{nr2} = 0 \tag{3.2}$$

$$k_1 A_r + k_2 A_{nl} - k_1 A_{in} = -k_3 A_t - k_4 A_{nr} + k_3 A_{r2} + k_4 A_{nr2} \tag{3.3}$$

$$\begin{aligned} &D_1\left[(k_1^2 - \nu_1 k_n^2)A_r + (k_2^2 - \nu_1 k_n^2)A_{nl} + (k_1^2 - \nu_1 k_n^2)A_{in}\right] = \\ &D_2\left[(k_3^2 - \nu_2 k_n^2)A_t + (k_4^2 - \nu_2 k_n^2)A_{nr} + (k_3^2 - \nu_2 k_n^2)A_{r2} + (k_4^2 - \nu_2 k_n^2)A_{nr2}\right]. \end{aligned} \tag{3.4}$$

In addition to equations (2.8)-(2.10), two further boundary conditions at the right-hand free edge of plate 2 are included.

(1) bending moment at the right-hand edge of plate 2:

$$M_{xx,2}(L_2, y) = D_2\left\{\frac{\partial^2 w_2}{\partial x^2} + \nu_2 \frac{\partial^2 w_2}{\partial y^2}\right\}_{x=L_2} = 0. \tag{3.5}$$

(2) shear force at the right-hand edge of plate 2:

$$F_2(L_2, y) = -D_2\left\{\frac{\partial^3 w_2}{\partial x^3} - (2-\nu_2)k_n^2 \frac{\partial w_2}{\partial x}\right\}_{x=L_2} = 0. \tag{3.6}$$

Substituting equation (3.1) into equations (3.5) and (3.6), then

$$(k_3^2 - \nu_2 k_n^2)e^{-k_3 L_2} A_t + (k_4^2 - \nu_2 k_n^2)e^{-k_4 L_2} A_{nr} + (k_3^2 - \nu_2 k_n^2)e^{k_3 L_2} A_{r2} + (k_4^2 - \nu_2 k_n^2)e^{k_4 L_2} A_{nr2} = 0 \tag{3.7}$$

$$\begin{aligned} &k_3\left\{-k_3^2 + (2-\nu_2)k_n^2\right\}e^{-k_3 L_2} A_t + k_4\left\{-k_4^2 + (2-\nu_2)k_n^2\right\}e^{-k_4 L_2} A_{nr} + \\ &k_3\left\{k_3^2 - (2-\nu_2)k_n^2\right\}e^{k_3 L_2} A_{r2} + k_4\left\{k_4^2 - (2-\nu_2)k_n^2\right\}e^{k_4 L_2} A_{nr2} = 0. \end{aligned} \tag{3.8}$$

Equations (2.12), (3.2)-(3.4) and (3.7)-(3.8) can be written in matrix form,

$$\boldsymbol{B}_2 \boldsymbol{A}_2 = \boldsymbol{C}_2 \tag{3.9}$$

where

$$\boldsymbol{B}_2 = \begin{bmatrix} 1 & 1 & 0 & 0 & 0 & 0 \\ 0 & 0 & 1 & 1 & 1 & 1 \\ k_1 & k_2 & k_3 & k_4 & -k_3 & -k_4 \\ D_1(k_1^2 - \nu_1 k_n^2) & D_1(k_2^2 - \nu_1 k_n^2) & -D_2(k_3^2 - \nu_2 k_n^2) & -D_2(k_4^2 - \nu_2 k_n^2) & -D_2(k_3^2 - \nu_2 k_n^2) & -D_2(k_4^2 - \nu_2 k_n^2) \\ 0 & 0 & (k_3^2 - \nu_2 k_n^2)e^{-k_3 L_2} & (k_4^2 - \nu_2 k_n^2)e^{-k_4 L_2} & (k_3^2 - \nu_2 k_n^2)e^{k_3 L_2} & (k_4^2 - \nu_2 k_n^2)e^{k_4 L_2} \\ 0 & 0 & k_3\left\{-k_3^2 + (2-\nu_2)k_n^2\right\}e^{-k_3 L_2} & k_4\left\{-k_4^2 + (2-\nu_2)k_n^2\right\}e^{-k_4 L_2} & k_3\left\{k_3^2 - (2-\nu_2)k_n^2\right\}e^{k_3 L_2} & k_4\left\{k_4^2 - (2-\nu_2)k_n^2\right\}e^{k_4 L_2} \end{bmatrix} \tag{3.10}$$

$$\boldsymbol{A}_2 = \left[\frac{A_r}{A_{in}} \quad \frac{A_{nl}}{A_{in}} \quad \frac{A_t}{A_{in}} \quad \frac{A_{nr}}{A_{in}} \quad \frac{A_{r2}}{A_{in}} \quad \frac{A_{nr2}}{A_{in}} \right]^T \tag{3.11}$$

and $$\boldsymbol{C}_2 = \left[-1 \quad 0 \quad -k_1 \quad -D_1(k_1^2 - \nu_1 k_n^2) \quad 0 \quad 0 \right]^T . \tag{3.12}$$

The reflection efficiency r and the transmission efficiency τ can be obtained from

$$r = \left| \frac{A_r}{A_{in}} \right|^2 \tag{3.13}$$

$$\tau = 1 - r . \tag{3.14}$$

In this model, it is assumed that there is no damping in the semi-infinite source plate, as before, whereas the finite receiver plate is damped with a loss factor, η. This loss factor makes the bending wavenumber complex. The transmitted wave at the joint is propagated to the far edge of the receiver plate and then reflected back towards the joint. If there were no damping in the receiver plate, all the power flowing into the receiver plate would be reflected out of it again and τ would be zero.

Figure 3.2.(a) shows results for an example case, a semi-infinite source plate (thickness 3 mm, finite width 1 m) coupled to a finite receiver plate (thickness 2 mm, length 1 m) for $n = 1$. At low frequencies, the transmission efficiency oscillates considerably around that for two semi-infinite plates, whereas it converges to that for two semi-infinite plates as frequency increases. The peaks and troughs in the transmission efficiency are related to the modal behaviour of the receiver plate. This issue is discussed further in the following section. Figure 3.2.(b) shows the effective CLF for n = 1 estimated by equation (2.22) when the length of the source plate is 0.5 m.

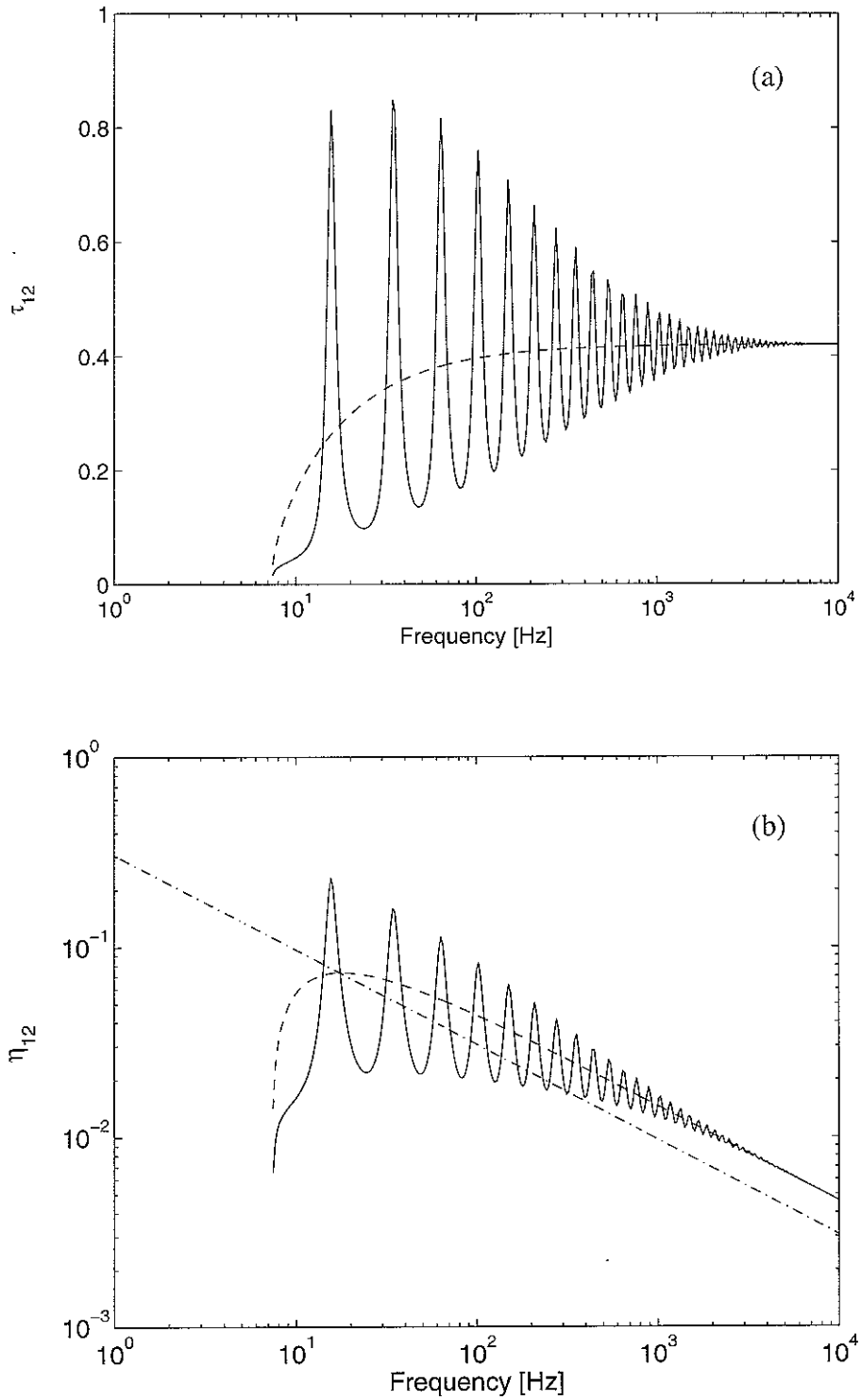

Figure 3.2. (a) Transmission efficiency τ_{12} for a semi-infinite plate (thickness $h_1 = 3$mm) of finite width ($b = 1$m) coupled to a finite plate (thickness $h_2 = 2$mm, length $L_2 = 1$m) for $n = 1$; the damping loss factor ($\eta_1 = 0$, $\eta_2 = 0.1$); —, semi-infinite to finite plates; ---, two semi-infinite plates of finite width; (b) CLF obtained from τ_{12} for source plate of length 0.5 m; —, semi-infinite to finite plates; ---, two semi-infinite plates of finite width; -·-, two semi-infinite plates.

3.2 The influence of the modal behaviour of the finite receiver plate

The transmission efficiencies vary with the thickness ratio of the source and receiver plates. First, the thicknesses of the source plate are varied between 3 and 1/3 times the thickness of the finite receiver plate, which is fixed as 2 mm. Next, the thickness of the receiver plate is varied in the same range relative to the thickness of the semi-infinite source plate, which is fixed as 3 mm. Figure 3.3 shows the transmission efficiencies for these thickness ratios. The transmission efficiency tends to a maximum asymptotic value when the thicknesses of the two plates are equal and to a minimum when the ratio is largest or smallest. At high frequencies, the transmission efficiency for this model (the semi-infinite plate coupled to the finite plate) converges to that for two semi-infinite plates of finite width as seen in Figure 3.2.

The frequency of the peaks for the former case (varying the thicknesses of the source plate) remains essentially invariant as the thickness ratio varies (see Figure 3.3.(a)), whereas the peaks for the latter case (varying the thicknesses of the receiver plate) are shifted according to the modal behaviour of the receiver plate (see Figure 3.3.(b)). In order to study the influence of the modal behaviour, the natural frequencies of the uncoupled receiver plate are summarised in Table 3.1. Results are given for two sets of boundary conditions on the edge normally coupled to the infinite plate (simply supported or clamped).

The peaks in the transmission efficiency are found to occur between the natural frequencies of the uncoupled finite plate with either simply supported or clamped boundary condition at the interface, *i.e.* F-S-S-S or F-S-C-S, as shown in Figure 3.4. At resonances of the finite plate, the wave impedance of the receiver plate is low, producing a maximum in the transmitted energy, and hence in the power dissipated in the receiver plate. At anti-resonances of the receiver plate, the transmission efficiency has a minimum.

To investigate the influence of the modal behaviour of the finite receiver plate, here the thickness of the receiver plate is fixed as $h_2 = 2$ mm. When the thickness ratio h_1/h_2 is large, the infinite plate constrains the finite plate and the peaks tend towards the natural frequencies for a clamped edge [F-S-C-S]; when the ratio h_1/h_2 is small the peaks tend towards those for a simply supported edge [F-S-S-S] (see Figure 3.5).

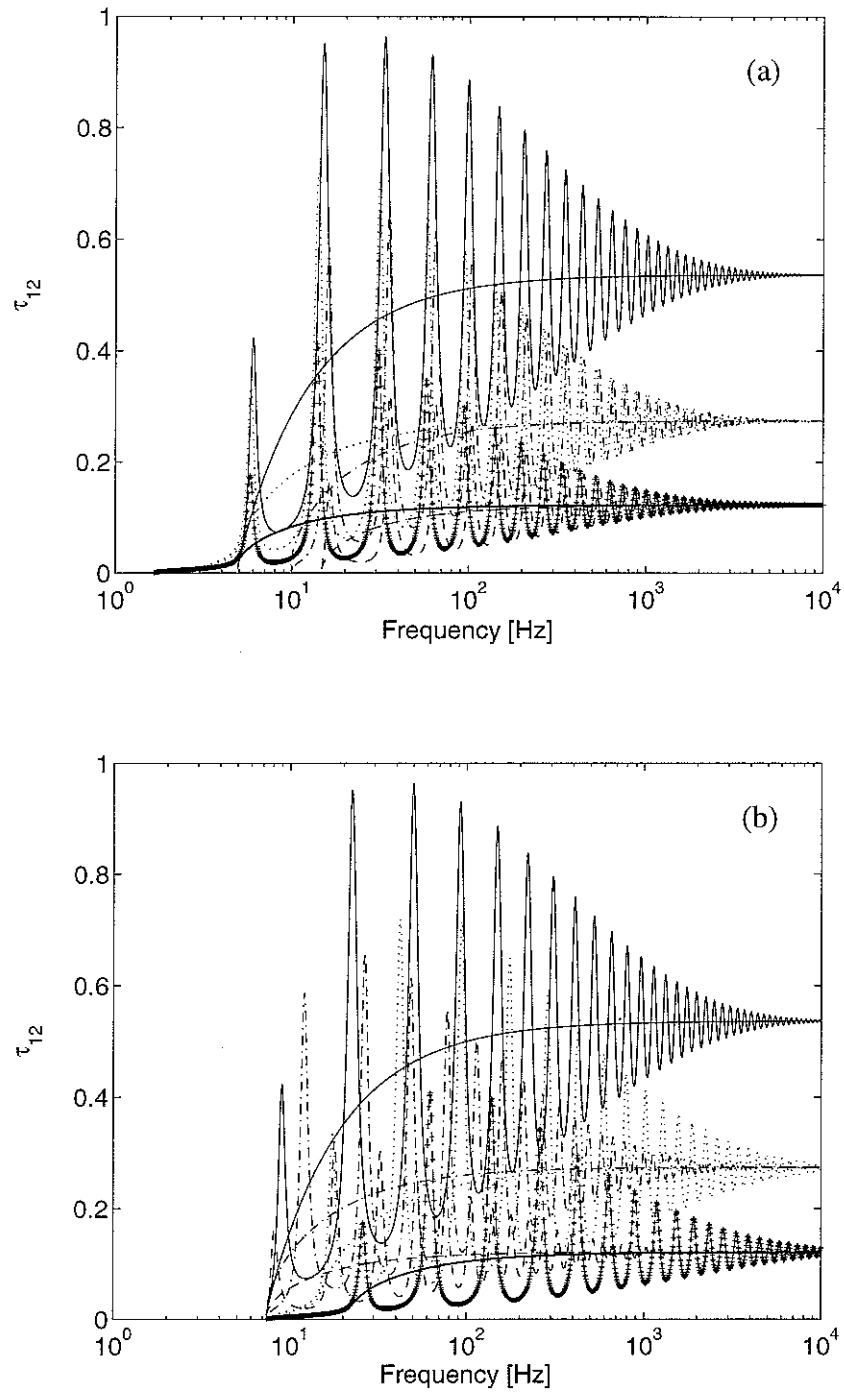

Figure 3.3. Transmission efficiencies for a semi-infinite source plate to a finite plate (width b = 1m, length L_2 = 1m) for different values of h_1/h_2 (a) h_2 fixed as 2 mm and (b) h_1 is fixed as 3 mm; ---, $h_1/h_2 = 3$; _._, $h_1/h_2 = 2$; ___, $h_1/h_2 = 1$; ...., $h_1/h_2 = 1/2$; -+-, $h_1/h_2 = 1/3$.

Table 3.1. The natural frequencies of the uncoupled receiver plate (width $b = 1$ m, length $L_2 = 1$ m, $n = 1$) with 3 simply supported edges and one free edge [F-S-S-S] and with 2 simply supported edges, one clamped edge and one free edge [F-S-C-S].

Thickness h_2 (mm)	F-S-S-S (Hz)	F-S-C-S (Hz)
2	5.74, 13.7, 30.4, 57.0, 93.5	6.20, 16.3, 35.6, 65.3, 104
1	2.87, 6.83, 15.2, 28.6, 47.0	3.11, 8.17, 17.8, 32.5, 51.8
1.5	4.28, 10.3, 22.8, 42.8, 69.8	4.66, 12.2, 26.7, 48.7, 78.1
3	8.64, 20.4, 45.8, 85.4, 140	9.32, 24.4, 53.3, 97.8, 155
6	17.2, 41.2, 91.4, 171, 281	18.7, 48.7, 107, 195, 311
9	25.8, 61.3, 137, 257, 421	28.1, 73.0, 160, 291, 469

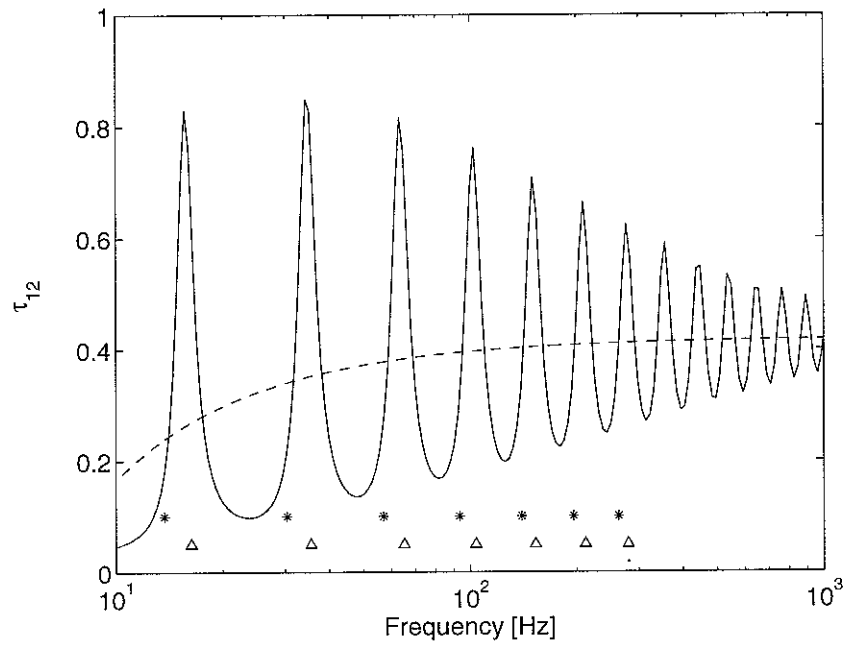

Figure 3.4. The transmission efficiency for an infinite source plate (width $b = 1$ m, $L_1 = 0.5$ m, $h_1 = 3$ mm) coupled to a finite receiver plate (width $b = 1$ m, $L_2 = 1$ m, $h_2 = 2$ mm) and two semi-infinite plates for $n = 1$; —, semi-infinite to finite; ---, semi-infinite to semi-infinite; natural frequencies of finite plate; *, F-S-S-S; Δ, F-S-C-S.

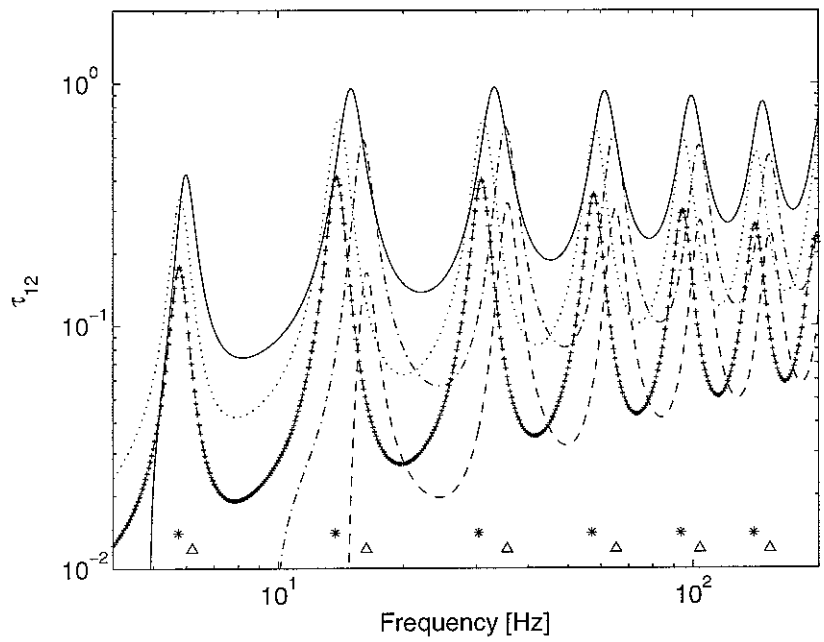

Figure 3.5. The transmission efficiencies for an infinite source plate coupled to a finite receiver plate with $b = 1$ m, $L_2 = 1$ m, $n = 1$, $h_2 = 2$ mm, for different values of h_1/h_2; ---, $h_1/h_2 = 3$; $^{-\cdot-}$, $h_1/h_2 = 2$; —, $h_1/h_2 = 1$; $^{\cdots}$, $h_1/h_2 = 1/2$; -+-, $h_1/h_2 = 1/3$; natural frequencies of finite plate; $*$, F-S-S-S; Δ, F-S-C-S.

3.3 The influence of damping of the receiver plate

It is assumed that there is no damping in the semi-infinite source plate, but the finite receiver plate is damped with a loss factor η. As damping of the receiver plate increases, more energy is absorbed by the receiver plate and less energy is reflected back towards the joint. Likewise the transmission efficiency τ_{12} oscillates less and converges more quickly to that for semi-infinite plates of finite width, as shown in Figure 3.6.

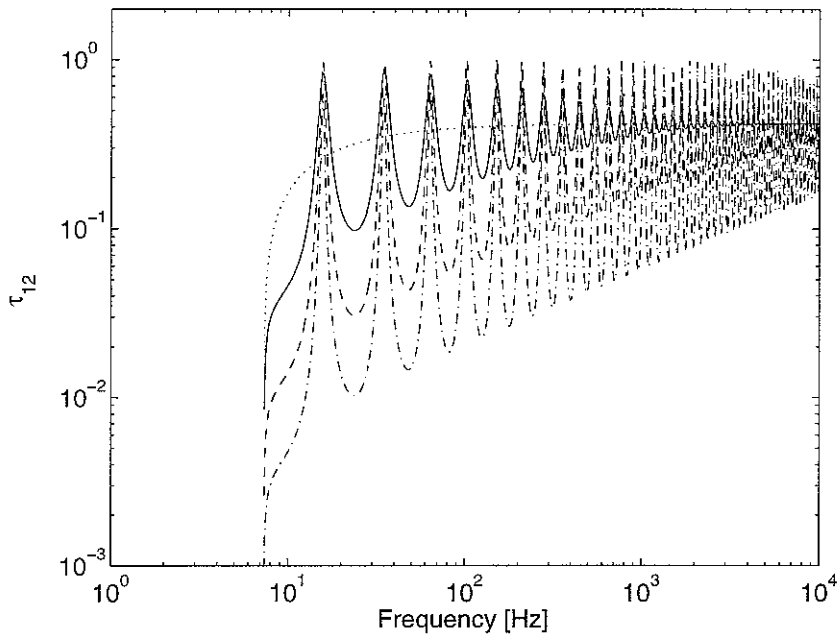

Figure 3.6 The influence of damping on the transmission efficiency for a semi-infinite plate (thickness $h_1 = 3$mm) of finite width ($b = 1$m) coupled to a finite plate (thickness $h_2 = 2$mm, length $L_2 = 1$m) for $n = 1$; —, $\eta_2 = 0.1$; ---, $\eta_2 = 0.03$; –·–, $\eta_2 = 0.01$; ·····, semi-infinite plates of finite width.

4. FINITE SOURCE PLATE COUPLED TO A SEMI-INFINITE RECEIVER PLATE OF FINITE WIDTH

4.1 Model

In order to evaluate the influence of the modal behaviour of the source plate on the coupling loss factor, one can consider a finite plate connected to a semi-infinite plate, as shown in Figure 4.1.

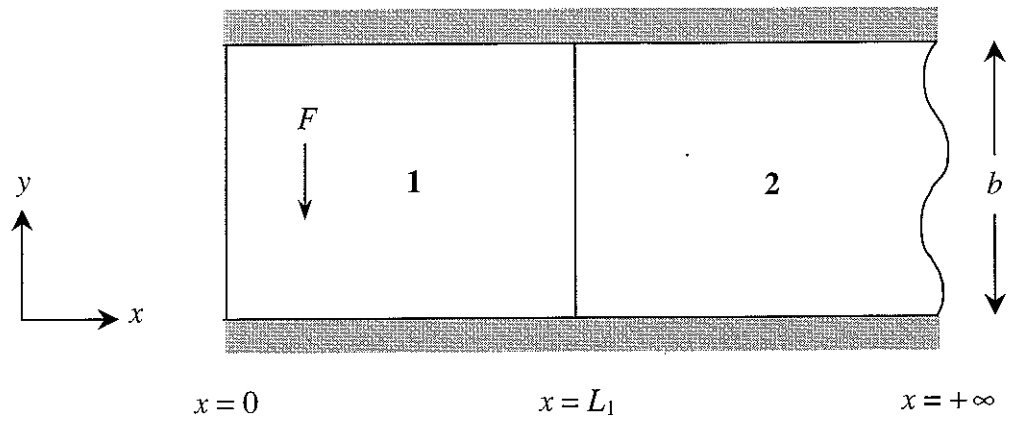

Figure 4.1 Finite (source) plate connected to a semi-infinite (receiver) plate of finite width b.

For this system, it is more appropriate to simulate a "rain-on-the-roof" type excitation rather than a propagating source wave as in the previous chapters. In a previous investigation on two finite plates [2], it has been shown that one needs of the order of 400 excitation points in the finite source plate to obtain reliable results, independent of the forcing points. Single point excitation is therefore applied at 400 randomly chosen points, avoiding edges. For each point force, this excites vibration in many different transverse orders, n, across the plate width. For a given frequency, all such components need to be included whose cut-on frequency is below the frequency under consideration.

The equations of motion are solved using a dynamic stiffness approach [5]. A harmonic point force is applied inside one plate. Thus the source plate is separated into two at the longitudinal position of the applied force. The dynamic stiffness matrices for the source plate, $\mathbf{K}_1$ and $\mathbf{K}_2$, are as given in [5]. For the semi-infinite plate, a dynamic stiffness matrix $\mathbf{K}_{inf}$ (see Appendix A) can be defined in terms of the positive-going nearfield and propagating waves at

the interface. The global dynamic stiffness matrix of the total system can be derived by assembling the dynamic stiffness matrices of the two finite plates and the semi-infinite plate and applying the continuity and equilibrium conditions at the interface. This global dynamic stiffness matrix $\mathbf{K}_{tot}$ can be reduced using a transformation matrix. The reduced dynamic stiffness matrix $\mathbf{K}$, for flexural motion only, is a 6×6 frequency-dependent matrix. The response can be obtained from $\mathbf{K}^{-1}\mathbf{F}$ for every frequency, where $\mathbf{F}$ is an applied force vector.

4.2 Coupling loss factor

The coupling loss factor (CLF) can be determined from the power balance equation [2]

$$\bar{P}^1_{1,\text{in}} = \bar{P}^1_{1,\text{diss}} + \bar{P}^1_{12} = \omega\left(\eta_1 \bar{E}^1_1 + \eta^1_{12}\bar{E}^1_1 - \eta^1_{21}\bar{E}^1_2\right) \tag{4.1}$$

where P_{in} and P_{diss} are the time-averaged input and dissipated powers, P_{12} is the net transmitted power from plate 1 to 2, η_1 is the internal loss factor of plate 1, E_1 and E_2 are the total time-averaged energies, η_{12} and η_{21} are the coupling loss factors. The superscript 1 means the excitation is applied to plate 1 and " $\bar{}$ " denotes an ensemble averaged quantity. As before, no damping is included in the semi-infinite plate. Due to its infinite nature, energy is only transmitted away from the joint and the term $\omega\eta_{21}\bar{E}^1_2$ representing power transmitted from plate 2 to plate 1, is zero. Since $\bar{P}^1_{1,\text{diss}} = \omega\eta_1\bar{E}^1_1$, the effective CLF for a particular finite source plate is obtained from

$$\hat{\eta}_{12} = \frac{P_{12}}{\omega E_1} = \eta_1 \frac{P_{12}}{P_{1,diss}}. \tag{4.2}$$

To evaluate the effective CLF, one needs to calculate the strain energy of the source plate E_1 and the power transmitted at the joint P_{12}. The response of the source plate is integrated analytically to give an accurate measure of its strain energy (see Appendix B). The transmitted power at the interface P_{12} is obtained directly from

$$P_{12} = \frac{1}{2}\text{Re}\left\{\sum_n \int_0^b M_n^*(y)\{j\omega\varphi_n(y)\}dy\right\} \tag{4.3}$$

where M_n is the internal moment amplitude / unit length at the interface calculated from the dynamic stiffness matrix and φ_n is the rotation amplitude. These are calculated for each transverse order n, integrated along the interface length b, and then summed.

The power dissipated and power transmitted for this system fluctuate due to the modal behaviour of the finite source plate, as shown in Figure 4.2. However the peaks in the two curves tend to coincide. The power transmitted becomes significantly lower than the power dissipated as frequency increases.

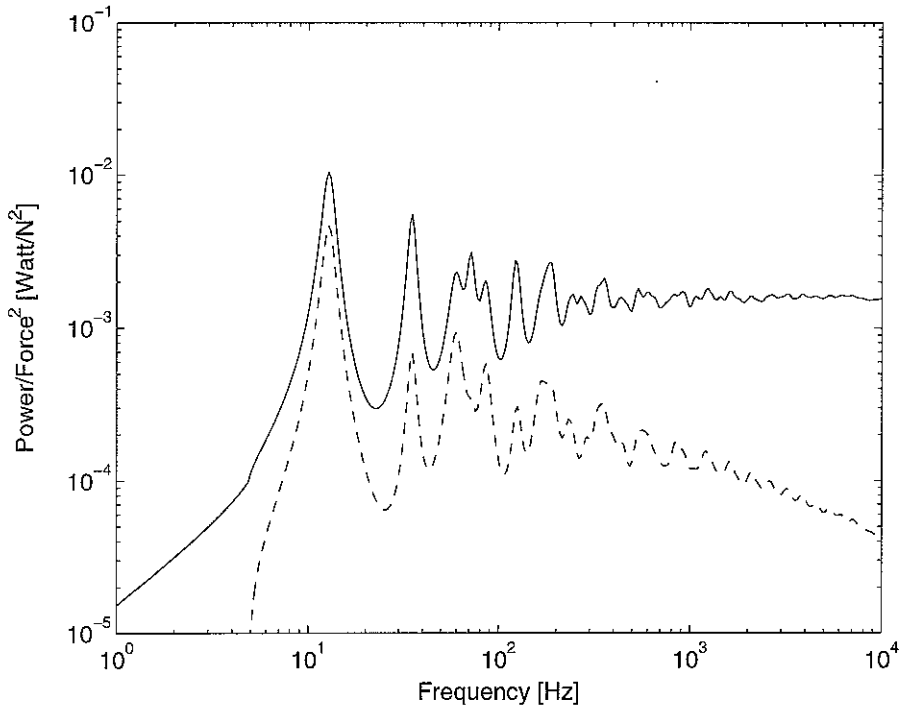

Figure 4.2 The power dissipated $P_{1,\,diss}$ and power transmitted P_{12} for a finite source plate (h_1 = 3mm, L_1 = 0.5m, η_1 = 0.1) coupled to a semi-infinite receiver plate (h_2 = 2mm, η_2 = 0) of finite width (b = 1m); —, $P_{1,\,diss}$; ---, P_{12}.

The effective CLF for a finite plate coupled to a semi-infinite plate of finite width (b = 1m) can be obtained from equation (4.2). Figure 4.3.(a) shows the effective CLF for transverse order n = 1 up to 4 which is averaged over 400 forcing points. Figure 4.3.(b) shows the result for n = 1 to $n_{\max}$, which is included whose cut-on frequency is below the frequency considered. At low frequencies, the effective CLF fluctuates around that obtained from two semi-infinite plates. As transverse order n increases and the sum over $n_{\max}$ is taken, the effective CLF converges to the CLF for two semi-infinite plates. However, the effective CLF is relatively smooth compared to the fluctuations in the CLF for a semi-infinite source plate coupled to a finite receiver plate (see Figure 3.2.(b)).

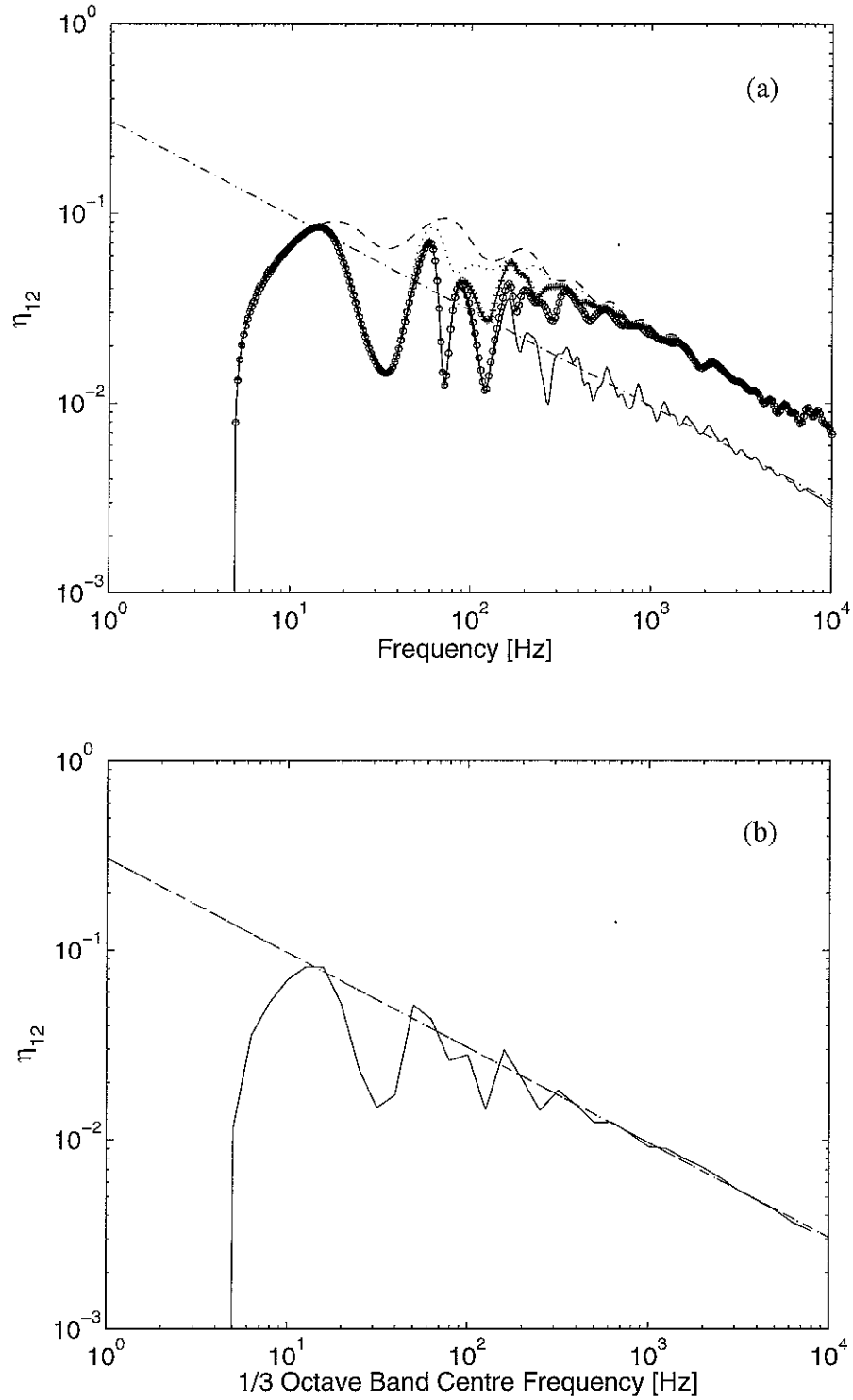

Figure 4.3. Effective CLF for finite source plate ($h_1 = 3$mm, $L_1 = 0.5$m, $\eta_1 = 0.1$) coupled to a semi-infinite receiver plate ($h_2 = 2$mm, $\eta_2 = 0$) of finite width ($b = 1$m); (a) η_{12} versus narrow frequency band and (b) η_{12} versus 1/3 octave frequency band; ---, $n = 1$; ····, $n = 1+2$; -·-, $n = 1+2+3$; -o-, $n = 1+2+3+4$; —, $n = 1$ up to 46; -·-, $\eta_{12\infty}$.

4.3 The influence of damping of the source plate

As damping of the source plate increases, the level of peaks in the power transmitted P_{12} and the energy E_1 decreases, as shown in Figure 4.4. However damping has only a small effect on the effective CLF, as shown in Figure 4.5.

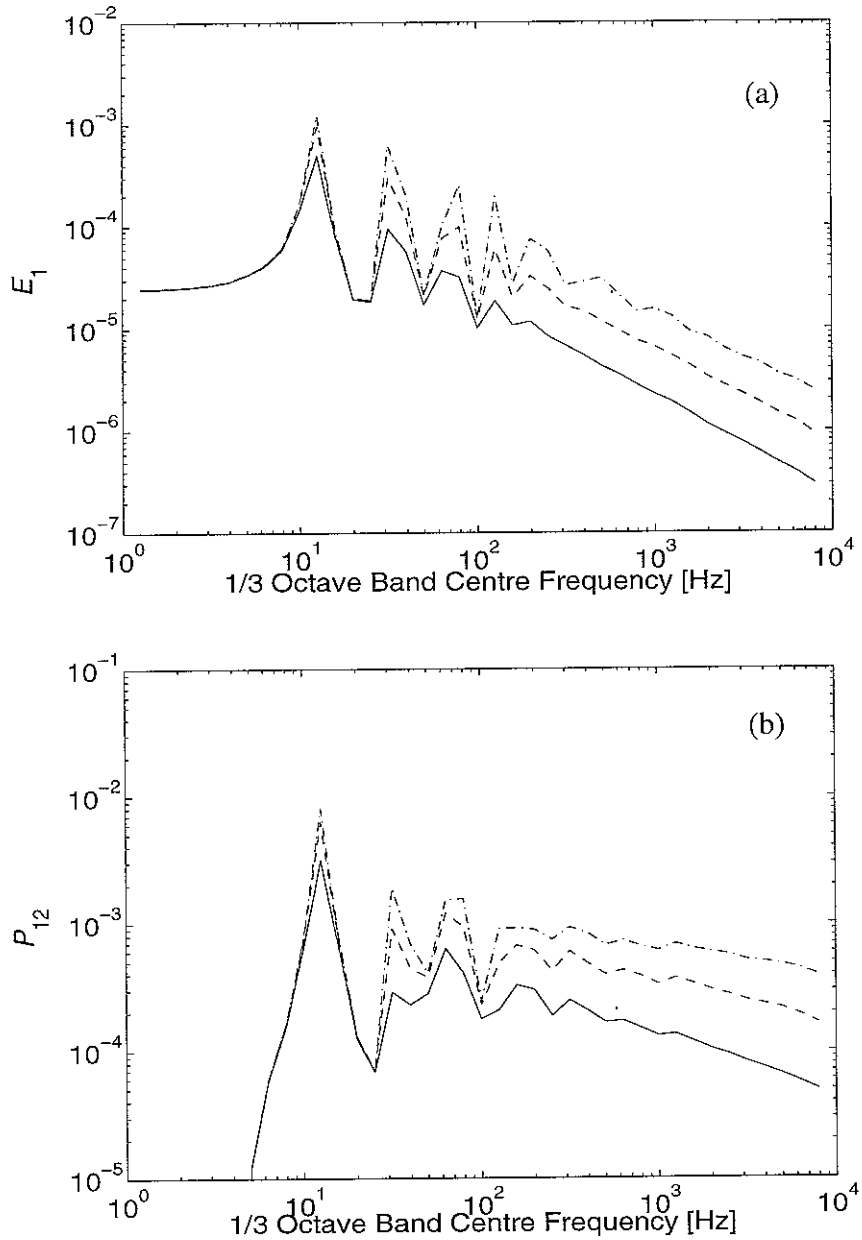

Figure 4.4 The influence of damping of the source plate on: (a) the transmitted power P_{12} and (b) the strain energy for the source plate E_1 for different damping loss factors; —, $\eta_1 = 0.1$; ---, $\eta_1 = 0.03$; -·-, $\eta_1 = 0.01$. The dimensions of the source and receiver plates are the same as Figure 4.3.

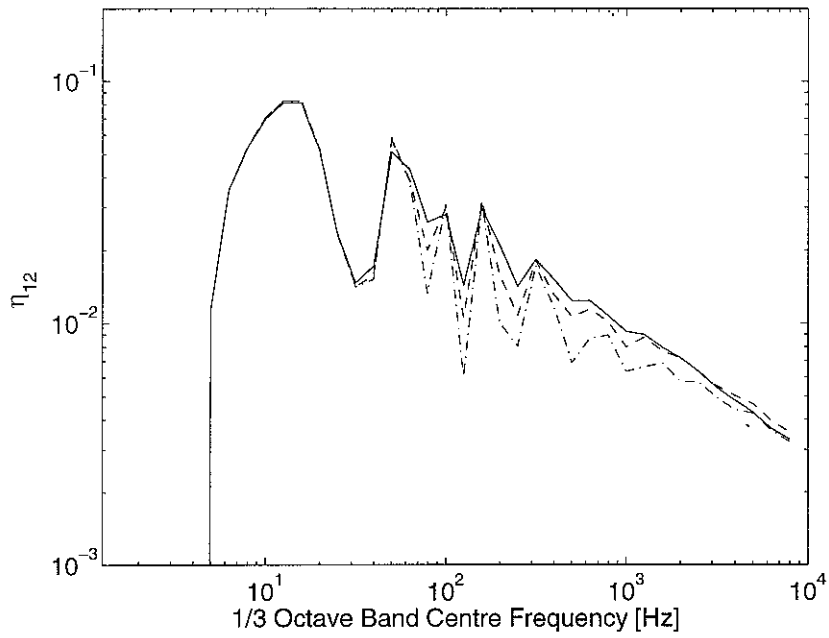

Figure 4.5 The influence of damping on the effective CLF for a finite source plate (h_1 = 3mm, L_1 = 0.5m, η_1 = 0.1) coupled to a semi-infinite receiver plate (h_2 = 2mm, η_2 = 0) of finite width (b = 1m) ; —, η_1 = 0.1; ---, η_1 = 0.03; -·-, η_1 = 0.01.

4.4 The influence of the modal behaviour of the finite source plate

This section investigates the influence of the modal behaviour of the finite source plate on the energy transmission in terms of the effective CLF. A parameter study is performed in which the thickness ratio between the two plates is varied and the modal behaviour of the finite source plate is examined.

First, the thicknesses of the finite source plate are varied between 3 and 1/3 times the thickness of the semi-infinite receiver plate, which is fixed as 2 mm. The influence of the thickness of the source plate is shown in Figure 4.6.(a). The peaks and troughs are related to the modal behaviour of the source plate. The natural frequencies for the uncoupled source plate are summarised in Table 4.1. Energy transmission starts at the cut-on frequency of the receiver plate whose thickness is kept the same, as indicated above. The maximum energy transmission occurs when the two plates have the same thicknesses.

Next, the thickness of the receiver plate is varied in the same range relative to the thickness of the finite source plate, which is fixed as 3 mm. The energy transmission varies as well, as the

thickness of the receiver plate is changed (see Figure 4.6.(b)). The peaks and troughs occur at similar frequencies, but these are related to the natural frequencies of the finite source plate (see Table 4.1) whose thickness is kept the same.

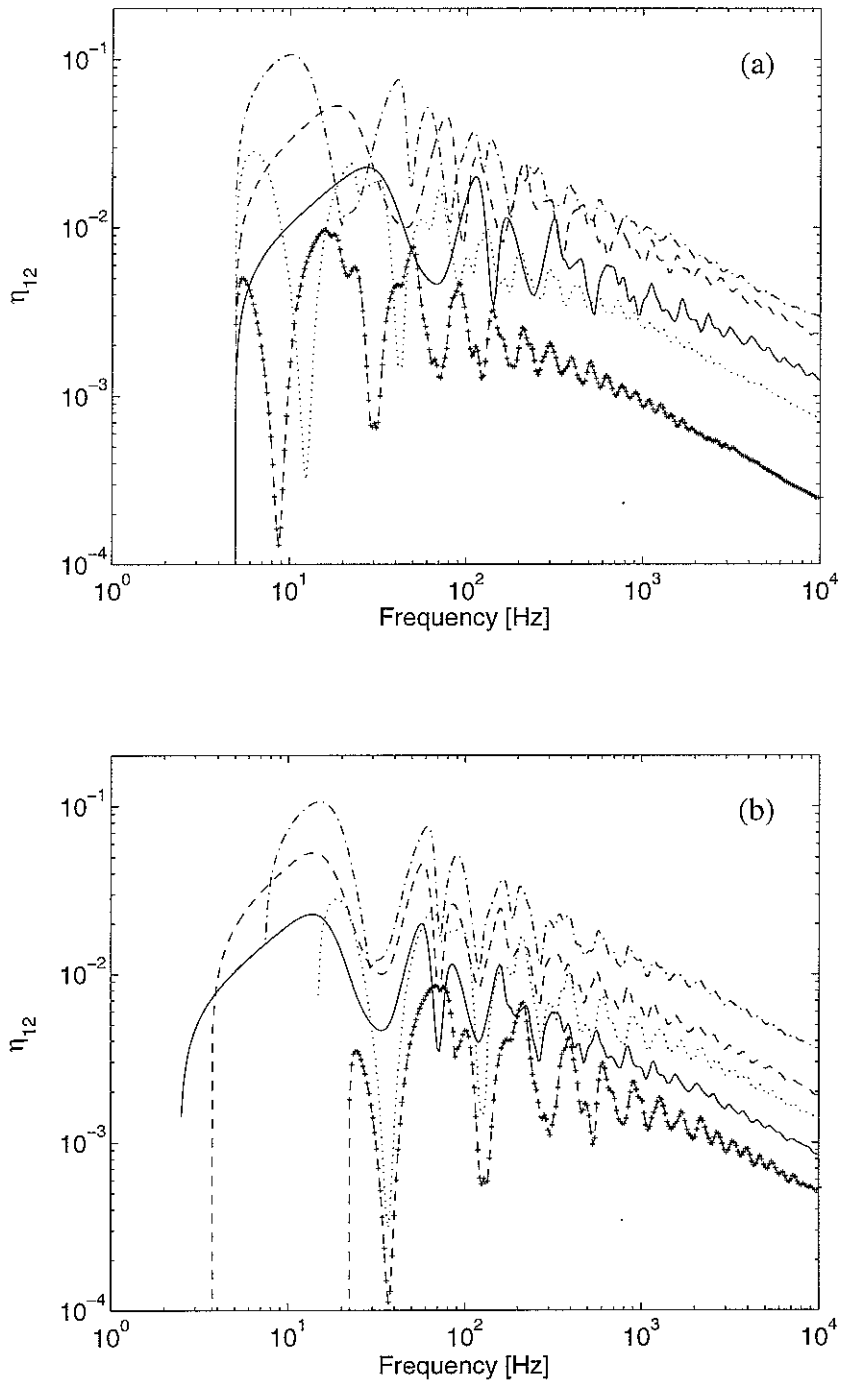

Figure 4.6. The effective CLFs for transmission from a finite source plate (width $b = 1$ m, length $L_1 = 0.5$ m) to an infinite receiver plate for different values of h_1/h_2; (a) h_2 is fixed as 2mm and (b) h_1 is fixed as 3mm; —, $h_1/h_2 = 3$; ---, $h_1/h_2 = 2$; -·-, $h_1/h_2 = 1$; ····, $h_1/h_2 = 1/2$; -·+-, $h_1/h_2 = 1/3$.

Table 4.1. The natural frequencies of the uncoupled source plate (width $b = 1$ m, length $L_1 = 0.5$ m, $n = 1$) with 3 simply supported edges and one free edge [F-S-S-S] and with 2 simply supported edges, one clamped edge and one free edge [F-S-C-S].

Thickness h_1 (mm)	F-S-S-S (Hz)	F-S-C-S (Hz)
6	23.6, 111, 314, 636, 1070	33.4, 148, 381, 728, 1200
4	15.8, 74.3, 210, 423, 714	22.3, 98.3, 254, 490, 799
2	7.88, 37.1, 105, 211, 358	11.1, 49.0, 127, 243, 399
1	3.95, 18.6, 39.5, 186, 524	5.58, 24.6, 63.6, 122, 200
0.7	2.61, 12.3, 35.0, 70.4, 119	3.72, 16.4, 42.5, 81.2, 134
3	11.8, 55.8, 157, 318, 536	16.8, 73.8, 191, 367, 602

To investigate the influence of the modal behaviour of the finite source plate in more detail, consider again the second case: the thickness of the finite source plate is fixed as $h_1 = 3$ mm and the thickness of the semi-infinite receiver plate is varied between 1/3 and 3 times the thickness of the finite source plate. The effective CLFs were shown in Figure 4.6.(b). The energy transmission starts at the cut-on frequency of the semi-infinite receiver plate. The effective CLF fluctuates at low frequencies and converges to the result of the infinite plate as shown in Figure 4.3. The peaks and troughs occur at similar frequencies as the thickness of the semi-infinite receiver plate varies. These peaks depend on the modal behaviour of the finite source plate, as the thickness of that plate is fixed. Table 4.2 presents the natural frequencies of an uncoupled source plate for different transverse orders, n and two different boundary conditions along the edge normally joined to plate 2.

Figure 4.7 compares these natural frequencies for two different boundary conditions and the effective CLFs for a finite source plate ($h_1 = 3$mm, length $L_1 = 0.5$ m) and semi-infinite receiver plate. These natural frequencies are shown for each n value. It is found that the first resonance corresponds to a peak in effective CLF, the second to a dip, the third to a peak and so on. The effective CLF for a finite source plate ((a) $h_1 = 3$mm, $h_2 = 2$mm, $L_1 = 0.5$ m and (b) $h_1 = 2$mm, and $h_2 = 3$mm, $L_1 = 1.0$ m) and semi-infinite receiver plate ($h_2 = 2$ mm), is compared with the CLF for two semi-infinite plates, for a diffuse field and for 4 transverse orders, in Figure 4.8. The troughs in the effective CLF correspond to the cut-on frequency of the source plate for $n>1$, which in turn correspond to the first resonance for a given n.

At a resonance of the finite plate, the effective angle of incidence is dominated by that corresponding to the mode. Consequently the effective CLF follows closely that for the semi-infinite plates with the corresponding order n. The fluctuations in effective CLF are therefore due to the predominance of particular angles of incidence, not due to the direct influence of the modal behaviour of the source plate.

Table 4.2. The natural frequencies of the uncoupled source plate (thickness $h_1 = 3.0$ mm, length $L_1 = 0.5$ m, width $b = 1$ m) with 3 simply supported edges and one free edge [F-S-S-S] and with 2 simply supported edges, one clamped edge and one free edge [F-S-C-S].

n	F-S-S-S (Hz)	F-S-C-S (Hz)
1	11.8, 55.8, 157, 318, 536, 812	16.8, 73.8, 191, 367, 602, 894
2	34.6, 82.2, 182, 342, 561, 840	37.3, 97.5, 215, 390, 624, 917
3	71.2, 122, 224, 384, 600, 876	72.8, 135, 253, 428, 662, 953
4	122, 175, 279, 439, 658, 930	123, 187, 306, 482, 716
5	188, 242, 348, 510, 730	189, 252, 372, 548, 783
6	267, 323, 431, 597, 812	269, 332, 453, 631, 864

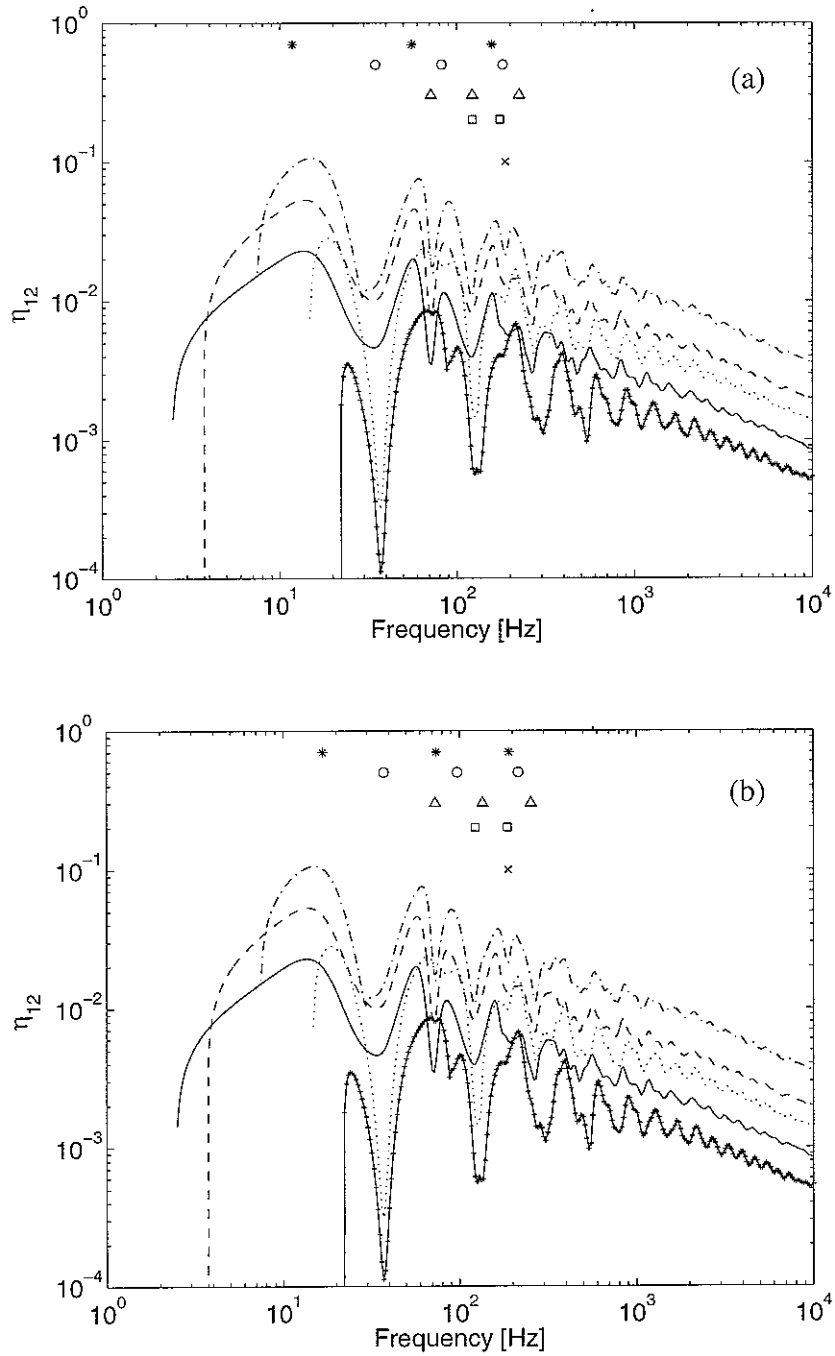

Figure 4.7. The effective CLFs for a finite plate ($L_1 = 0.5$ m, $h_1 = 3$ mm) coupled to a semi-infinite plate of finite width ($b = 1$ m); —, $h_2 = 1$mm; ---, $h_2 = 1.5$mm; $^{-}$ $^{-}$, $h_2 = 3$mm; ····, $h_2 = 6$mm; $^{-}$+$^{-}$, $h_2 = 9$mm; The symbols denote natural frequencies of finite source plate for different boundary conditions along the edge, (a) F-S-S-S and (b) F-S-C-S, and different transverse orders n; ∗, $n = 1$; o, $n = 2$; ∆, $n = 3$; □, $n = 4$; ×, $n = 5$.

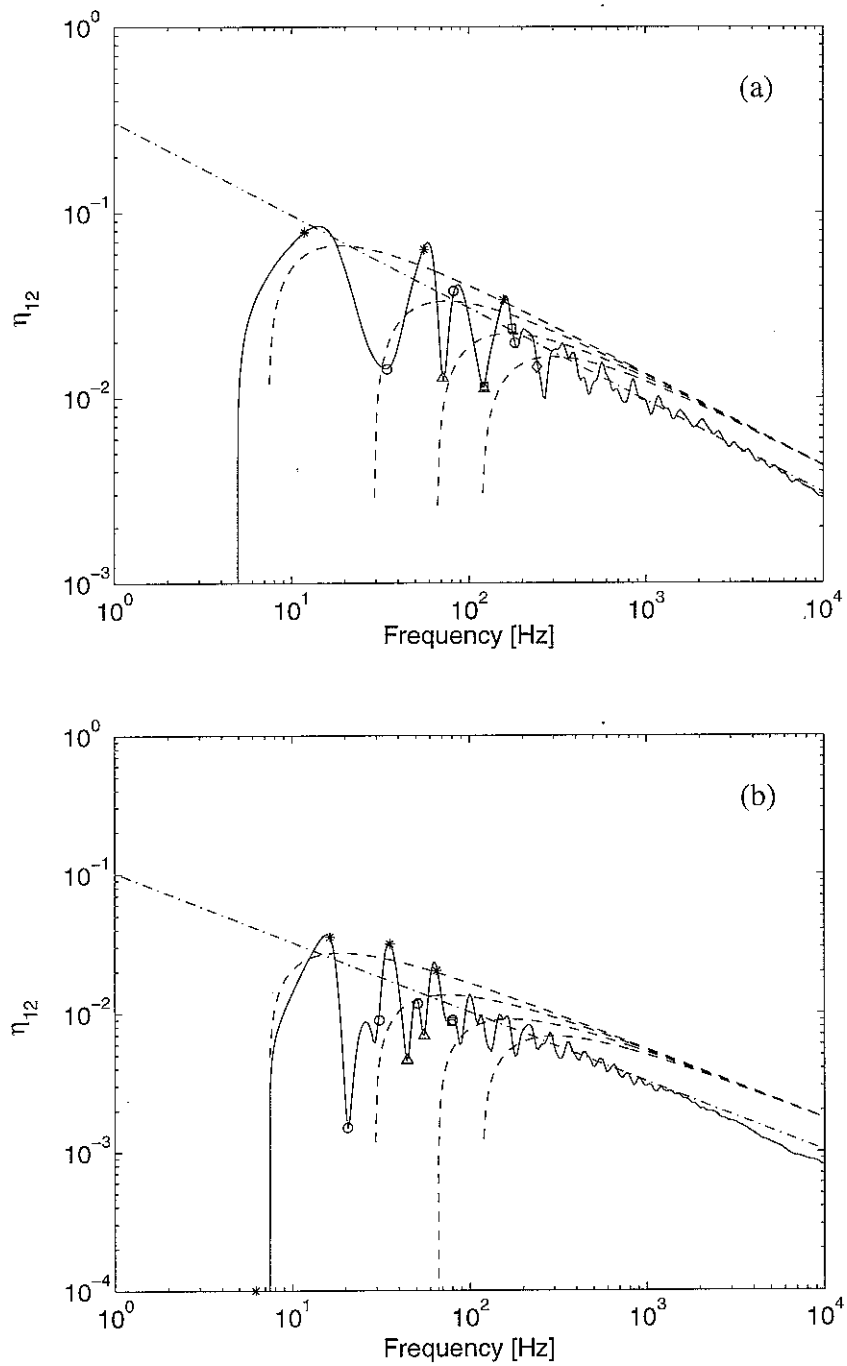

Figure 4.8. Comparison of the CLFs for a finite plate coupled to a semi-infinite plate of finite width, (a) $h_1 = 3$ mm, $h_2 = 2$ mm, $L_1 = 0.5$ m, and (b) $h_1 = 2$ mm, $h_2 = 3$ mm, $L_1 = 1.0$ m; –·–, the CLF for two semi-infinite plates; —, the effective CLF for a finite plate coupled to a semi-infinite plate of finite width($b = 1$ m); ---, the effective CLFs obtained from equation (2.22) for two semi-infinite plates of finite width ($n = 1$, 2, 3 and 4); The symbols denote natural frequencies of finite source plate for different boundary conditions along the edge, (a) F-S-S-S and (b) F-S-C-S, and different transverse orders n; $*$, $n = 1$; o, $n = 2$; $\triangle$, $n = 3$; $\square$, $n = 4$.

5. DISCUSSION

For finite coupled subsystems the variability due to modal behaviour in the effective coupling loss factor, or transmission efficiency, has been examined using a systematic investigation involving finite width semi-infinite plates and finite plates.

It was shown that the modal behaviour of both the source and receiver plates affects the energy transmission for two subsystems. Large variability in the energy transmission was found due to the modal behaviour of the receiver plate, with peaks occurring in the transmission efficiency at the receiver's resonances. Damping of the receiver plate controls the magnitude of these variations. However, smaller variations in the energy transmission can be attributed to the source subsystem characteristics, as produced in the finite source plate coupled to a semi-infinite receiver plate. This variation is due to the predominance of particular angles of incidence at a given frequency. Both peaks and troughs in the effective CLF correspond to natural frequencies of the uncoupled source plate. Damping of the source plate has only a small influence. Therefore it can be inferred that the modal overlap of the receiver plate is important whereas the modal density (not its damping) of the source plate is important. Figure 5.1 summarises these trends by comparing the CLFs found for a finite receiver or a finite source plate, taken from Figures 3.2.(b) and 4.3.(a).

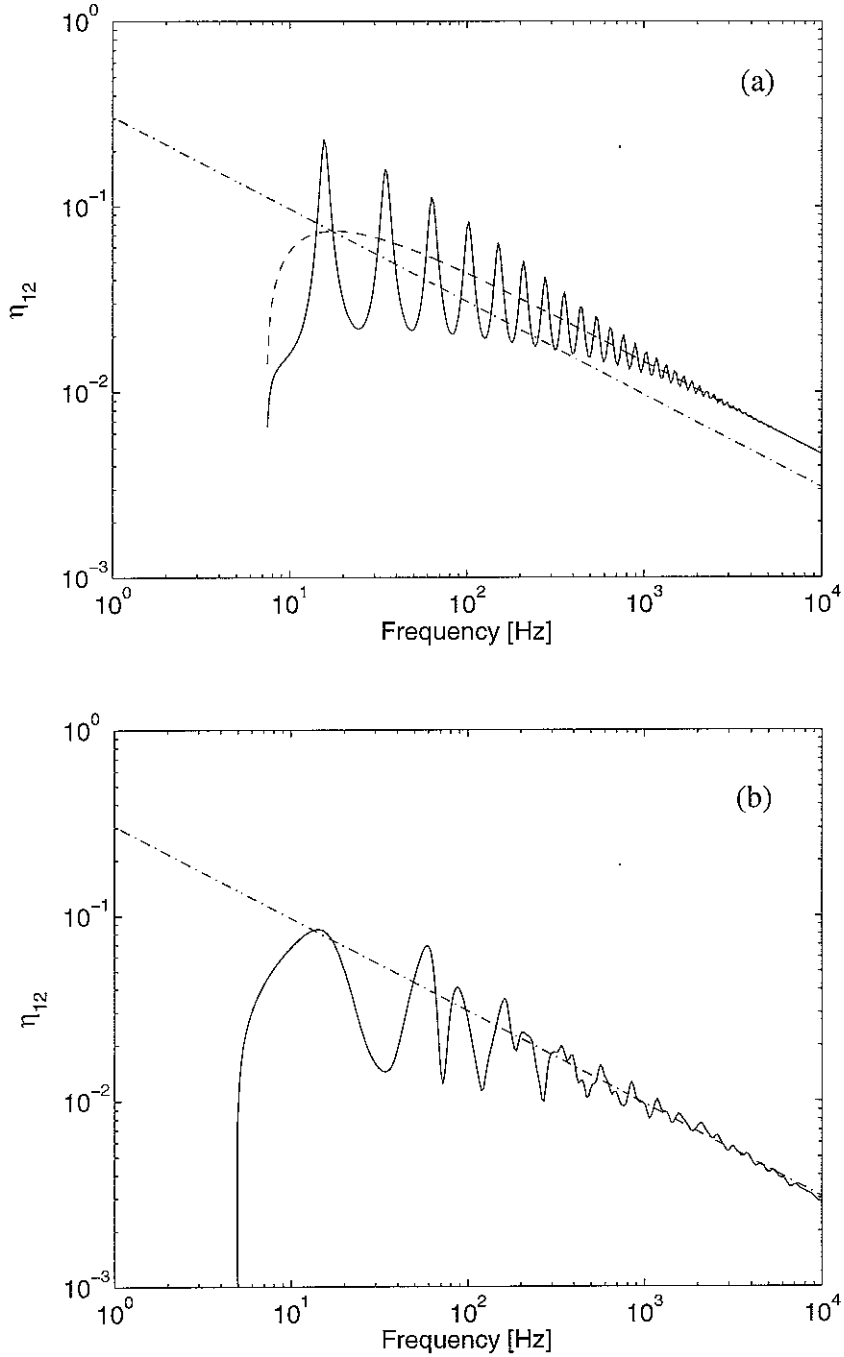

Figure 5.1. Comparison of the CLFs for two different models ($h_1 = 3$ mm, $h_2 = 2$ mm, $L_1 = 0.5$ m, $L_2 = 1.0$ m, $b = 1$ m); (a) semi-infinite source plate coupled to a finite receiver plate ($n = 1$) and (b) finite source plate coupled to a semi-infinite receiver plate ($n = 1$ up to 46); —, the effective CLF for model (a) or (b); -·-, the CLF for two semi-infinite plates; ---, the effective CLF obtained from equation (2.22) for two semi-infinite plates of finite width ($n = 1$).

REFERENCES

[1] L. Cremer, M. Heckl and E. E. Ungar 1988 *Structure-borne Sound: Structural Vibrations and Sound Radiation at Audio Frequencies*. New York: Springer-Verlag; second edition.

[2] W. S. Park, D. J. Thompson and N. S. Ferguson 2000 *ISVR Technical Memorandum* No.856, Sources of error and confidence intervals for SEA parameters of two coupled rectangular plates.

[3] R. J. M. Craik, J. A. Steel and D. I. Evans 1991 *Journal of Sound and Vibration* **144**(1), 95-107. Statistical energy analysis of structure-borne sound transmission at low frequencies.

[4] J. A. Steel and R. J. M. Craik 1994 *Journal of Sound and Vibration* **178**(4), 553-561. Statistical energy analysis of structure-borne sound transmission by finite element methods.

[5] W. S. Park, D. J. Thompson and N. S. Ferguson 1999 *ISVR Technical Memorandum* No.846, The power balance of beams and plates using the Dynamic Stiffness Method.

APPENDICES

A. Dynamic stiffness matrix for a semi-infinite plate

A semi-infinite plate, as shown in Figure A.1, is assumed to be simply supported along two opposite edges ($y = 0$ and $y = b$).

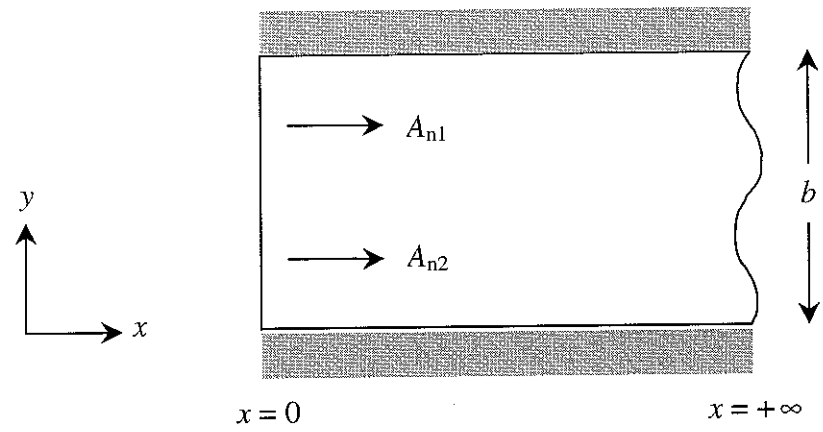

Figure A.1. A semi-infinite plate of finite width, b.

The deflection for flexural vibration may be taken to be of the form

$$W_n(x) = \sum_{r=1}^{2} A_{nr} e^{k_{nr} x} \tag{A.1}$$

where the A_{nr} terms are two unknown constants of integration which can be found by ensuring that the solution satisfies the boundary conditions at the left-hand edge of the plate and the k_{nr} terms are the positive-going nearfield and propagating waves ($k_{n1,n2} = -\sqrt{k_n^2 \pm k^2}$, $k = \left(\rho h \omega^2 / D\right)^{1/4}$ and $k_n = n\pi / b$).

Upon introducing the flexural displacement vector for longitudinal direction

$$\mathbf{u}_{nf}^T = \{W_n(0) \quad W_n'(0)\}, \tag{A.2}$$

then

$$\begin{aligned} W_n(0) &= A_{n1} + A_{n2} \\ W_n'(0) &= k_{n1} A_{n1} + k_{n2} A_{n2} \end{aligned} \tag{A.3}$$

or in matrix form

$$\mathbf{u}_{nf} = \begin{bmatrix} 1 & 1 \\ k_{n1} & k_{n2} \end{bmatrix} \begin{Bmatrix} A_{n1} \\ A_{n2} \end{Bmatrix} \tag{A.4}$$

$$\mathbf{u}_{nf} = \mathbf{p}_{1n}\mathbf{A}_n \tag{A.5}$$

where $\mathbf{A}_n^T = \{A_{n1} \quad A_{n2}\}$ and

$$\mathbf{p}_{1n} = \begin{bmatrix} 1 & 1 \\ k_{n1} & k_{n2} \end{bmatrix}. \tag{A.6}$$

Equation (A.1) may be used to derive a relationship between the displacements and forces at the left-hand end of the plate, and thus the dynamic stiffness matrix of the plate for flexural vibrations with transverse modeshape $\sin(k_n y)$ for each n. The longitudinal shear force $S_n(x)$ and bending moment $M_n(x)$ along the free edges may be written as [5]

$$S_n = -D\left[W_n''' - (2-\nu)k_n^2 W_n'\right] \tag{A.7}$$

$$M_n = -D\left[W_n'' - \nu k_n^2 W_n\right] \tag{A.8}$$

where D is the flexural rigidity ($= Eh^3/12(1-\nu^2)$) and ν is Poisson's ratio.

Upon introducing the restoring force vector

$$\mathbf{F}_{nf}^T = \{-S_n(0) \quad M_n(0)\} \tag{A.9}$$

where $$-S_n(0) = D\left[\sum_{r=1}^{2}(k_{nr})^3 A_{nr} - (2-\nu)k_n^2\left\{\sum_{r=1}^{2} k_{nr}A_{nr}\right\}\right] \tag{A.10}$$

and $$M_n(0) = -D\left[\sum_{r=1}^{2}(k_{nr})^2 A_{nr} - \nu k_n^2 \sum_{r=1}^{2} A_{nr}\right] \tag{A.11}$$

From equation (A.5), $\mathbf{A}_n = \mathbf{p}_{1n}^{-1}\mathbf{u}_{nf}$, equation (A.9) can be rewritten in matrix form,

$$\mathbf{F}_{nf} = \mathbf{p}_{2n}\mathbf{A}_n = \mathbf{p}_{2n}\mathbf{p}_{1n}^{-1}\mathbf{u}_{nf} = \mathbf{K}_{\text{inf}}\mathbf{u}_{nf} \tag{A.12}$$

$$\mathbf{K}_{\text{inf}} = \mathbf{p}_{2n}\mathbf{p}_{1n}^{-1} \tag{A.13}$$

and

$$\mathbf{p}_{2n} = \mathbf{D}\begin{bmatrix} (k_{n1})^3 - (2-\nu)k_n^2 k_{n1} & (k_{n2})^3 - (2-\nu)k_n^2 k_{n2} \\ -(k_{n1})^2 + \nu k_n^2 & -(k_{n2})^2 + \nu k_n^2 \end{bmatrix} \tag{A.14}$$

where $\mathbf{K}_{inf}$ is the dynamic stiffness matrix of the semi-infinite plate for flexural vibrations.

B. Analytical integration of strain energy

In calculating the energy of each plate, an analytical integration has been performed to give good agreement. The displacements and their derivatives are obtained from the dynamic stiffness approach.

B.1. The strain energy for flexural vibration

The strain energy for flexural vibration is given by [5]

$$U_f = \frac{D}{2}\int_0^b \int_0^L \left[\left(\frac{\partial^2 w}{\partial x^2} \right)^2 + \left(\frac{\partial^2 w}{\partial y^2} \right)^2 + 2\nu \frac{\partial^2 w}{\partial x^2}\frac{\partial^2 w}{\partial y^2} + 2(1-\nu)\left(\frac{\partial^2 w}{\partial x \partial y} \right)^2 \right] dxdy \qquad \text{(B.1)}$$

where D is the flexural rigidity ($= Eh^3/12(1-\nu^2)$, E is Young's modulus, h is the thickness of the plate, ν is Poisson's ratio, respectively), b is the width of the plate, L is the length of the plate and w is the out-of-plane deflection. In equation (B.1) w is a real quantity.

The out-of-plane displacement amplitude may be taken to be of the form

$$w(x, y) = \sum_{n=1}^{n_{max}} \sum_{m=1}^{4} A_{nm} e^{k_{nm} x} \sin(k_n y) \qquad \text{(B.2)}$$

where the complex A_{nm} terms are four unknown constants of integration which can be found by ensuring that the solution satisfies the boundary conditions at the ends. The k_{nm} terms are the four complex wavenumbers, k_n ($=n\pi y/b$) is the trace wavenumber in y direction and n is the number of half-sine waves along the transverse edge.

The first term of the integral in equation (B.1) can be rewritten in the form

$$\int_0^b \int_0^L \left| \frac{\partial^2 w}{\partial x^2} \right|^2 dxdy = \int_0^b \int_0^L \left(\frac{\partial^2 w}{\partial x^2} \right) \left(\frac{\partial^2 w}{\partial x^2} \right)^* dxdy \qquad \text{(B.3)}$$

where

$$\frac{\partial^2 w}{\partial x^2} = \sum_{n=1}^{n_{max}} \sum_{m=1}^{4} A_{nm} k_{nm}^2 e^{k_{nm} x} \sin(k_n y) \qquad \text{(B.4)}$$

and $*$ denotes the complex conjugate.

Substituting equation (B.4) into equation (B.3),

$$\int_0^b \int_0^L \left[\left(\sum_n \sum_m A_{nm} k_{nm}^2 e^{k_{nm} x} \right) \left(\sum_{n'} \sum_{m'} A_{n'm'}^* k_{n'm'}^{*2} e^{k_{n'm'}^* x} \right) \sin(k_n y) \sin(k_{n'} y) \right] dxdy$$
$$= \frac{b}{2} \sum_n \sum_m \sum_{m'} \frac{A_{nm} A_{nm'}^* k_{nm}^2 k_{nm'}^{*2}}{k_{nm} + k_{nm'}^*} \left\{ e^{(k_{nm} + k_{nm'}^*)L} - 1 \right\} \tag{B.5}$$

where $\int_0^b \sin(k_n y) \sin(k_{n'} y)\, dy = \frac{b}{2}$ if $n = n'$.

The second term of the integral in equation (B.1) can be rewritten as

$$\int_0^b \int_0^L \left| \frac{\partial^2 w}{\partial y^2} \right|^2 dxdy = \int_0^b \int_0^L \left(\frac{\partial^2 w}{\partial y^2} \right) \left(\frac{\partial^2 w}{\partial y^2} \right)^* dxdy \tag{B.6}$$

where
$$\frac{\partial^2 w}{\partial y^2} = -\sum_{n=1}^{n_{max}} \sum_{m=1}^{4} k_n^2 A_{nm} e^{k_{nm} x} \sin(k_n y). \tag{B.7}$$

Substituting equation (B.7) into equation (B.6),

$$\int_0^b \int_0^L \left[\left(-\sum_n \sum_m k_n^2 A_{nm} e^{k_{nm} x} \right) \left(-\sum_{n'} \sum_{m'} k_{n'}^2 A_{n'm'}^* e^{k_{nm} x} \right) \sin(k_n y) \sin(k_{n'} y) \right] dxdy$$
$$= \frac{b}{2} \sum_n \sum_m \sum_{m'} \frac{k_n^4 A_{nm} A_{nm'}^*}{k_{nm} + k_{nm'}^*} \left\{ e^{(k_{nm} + k_{nm'}^*)L} - 1 \right\} \tag{B.8}$$

The third term of the integral in equation (B.1) can be rewritten as

$$2\nu \int_0^b \int_0^L \mathrm{Re} \left[\left(\frac{\partial^2 w}{\partial x^2} \right) \left(\frac{\partial^2 w}{\partial y^2} \right)^* \right] dxdy \tag{B.9}$$

Substituting equations (B.4) and (B.7) into equation (B.9),

$$b\nu \int_0^b \int_0^L \mathrm{Re} \left[\left(\sum_n \sum_m A_{nm} k_{nm}^2 e^{k_{nm} x} \right) \left(-\sum_{n'} \sum_{m'} k_{n'}^2 A_{n'm'}^* e^{k_{n'm'} x} \right) \sin(k_n y) \sin(k_{n'} y) \right] dxdy$$
$$= -b\nu \sum_n \sum_m \sum_{m'} k_n^2 \, \mathrm{Re} \left[\frac{A_{nm} A_{nm'}^* k_{nm}^2}{k_{nm} + k_{nm'}^*} \left\{ e^{(k_{nm} + k_{nm'}^*)L} - 1 \right\} \right] \tag{B.10}$$

The last term of the integral in equation (B.1) can be rewritten as

$$2(1-\nu) \int_0^b \int_0^L \left| \frac{\partial^2 w}{\partial x \partial y} \right|^2 dxdy = 2(1-\nu) \int_0^b \int_0^L \left(\frac{\partial^2 w}{\partial x \partial y} \right) \left(\frac{\partial^2 w}{\partial x \partial y} \right)^* dxdy \tag{B.11}$$

where $$\frac{\partial^2 w}{\partial x \partial y} = \sum_{n=1}^{n_{max}} \sum_{m=1}^{4} k_n A_{nm} k_{nm} e^{k_{nm} x} \cos(k_n y). \quad \text{(B.12)}$$

Substituting equation (B.12) into equation (B.11),

$$\begin{aligned} & 2(1-\nu)\int_0^b \int_0^L \left[\left(\sum_n \sum_m k_n A_{nm} k_{nm} e^{k_{nm} x} \right) \left(\sum_{n'} \sum_{m'} k_{n'} A^*_{n'm'} k^*_{n'm'} e^{k^*_{n'm'} x} \right) \cos(k_n y) \cos(k_{n'} y) \right] dxdy \\ & = b(1-\nu) \sum_n \sum_m \sum_{m'} \frac{k_n^2 A_{nm} A^*_{nm'} k_{nm} k^*_{nm'}}{k_{nm} + k^*_{nm'}} \left\{ e^{(k_{nm} + k^*_{nm'})L} - 1 \right\} \end{aligned} \quad \text{(B.13)}$$

The strain energy for flexural vibration can be analytically obtained from equations (B.5), (B.8), (B.10) and (B.13).

$$\begin{aligned} U_f = \frac{Db}{4} \Bigg[& \sum_n \sum_m \sum_{m'} \frac{A_{nm} A^*_{nm'} k_{nm}^2 k^{*2}_{nm'}}{k_{nm} + k^*_{nm'}} \left\{ e^{(k_{nm} + k^*_{nm'})L} - 1 \right\} + \\ & \sum_n \sum_m \sum_{m'} \frac{k_n^4 A_{nm} A^*_{nm'}}{k_{nm} + k^*_{nm'}} \left\{ e^{(k_{nm} + k^*_{nm'})L} - 1 \right\} - \\ & 2\nu \sum_n \sum_m \sum_{m'} k_n^2 \, \mathrm{Re} \left[\frac{A_{nm} A^*_{nm'} k_{nm}^2}{k_{nm} + k^*_{nm'}} \left\{ e^{(k_{nm} + k^*_{nm'})L} - 1 \right\} \right] + \\ & 2(1-\nu) \sum_n \sum_m \sum_{m'} \frac{k_n^2 A_{nm} A^*_{nm'} k_{nm} k^*_{nm'}}{k_{nm} + k^*_{nm'}} \left\{ e^{(k_{nm} + k^*_{nm'})L} - 1 \right\} \Bigg] \\ = \frac{Db}{4} \mathrm{Re} \Bigg(& \sum_n \sum_m \sum_{m'} \frac{A_{nm} A^*_{nm'}}{k_{nm} + k^*_{nm'}} \left\{ e^{(k_{nm} + k^*_{nm'})L} - 1 \right\} \begin{Bmatrix} k_{nm}^2 k^{*2}_{nm'} + k_n^4 + 2\nu k_{nm}^2 + \\ 2(1-\nu) k_n^2 k_{nm} k^*_{nm'} \end{Bmatrix} \Bigg) \end{aligned} \quad \text{(B.14)}$$

B.2. The strain energy for in-plane vibration

The strain energy for in-plane vibration is given by [5]

$$U_i = \frac{Eh}{2(1-\nu^2)} \int_0^b \int_0^L \left[\left(\frac{\partial u}{\partial x} \right)^2 + \left(\frac{\partial v}{\partial y} \right)^2 + 2\nu \frac{\partial u}{\partial x} \frac{\partial v}{\partial y} + \frac{(1-\nu)}{2} \left(\frac{\partial u}{\partial y} + \frac{\partial v}{\partial x} \right)^2 \right] dxdy \quad \text{(B.15)}$$

where u and v are the longitudinal and transverse deflection, respectively.

If the boundary conditions are simply-supported along the longitudinal edges, the in-plane deflections, the longitudinal deflection u and the transverse deflection v, may be written as [5]

$$u(x,y)=\sum_{n=1}^{n_{max}}\left\{\begin{bmatrix}\lambda_{n1} & \lambda_{n2}\end{bmatrix}\begin{bmatrix}C_{n1}e^{\lambda_{n1}x}\\ C_{n2}e^{\lambda_{n2}x}\end{bmatrix}+\begin{bmatrix}k_n & k_n\end{bmatrix}\begin{bmatrix}C_{n3}e^{\lambda_{n3}x}\\ C_{n4}e^{\lambda_{n4}x}\end{bmatrix}\right\}\sin(k_n y) \tag{B.16}$$

$$v(x,y)=\sum_{n=1}^{n_{max}}\left\{\begin{bmatrix}k_n & k_n\end{bmatrix}\begin{bmatrix}C_{n1}e^{\lambda_{n1}x}\\ C_{n2}e^{\lambda_{n2}x}\end{bmatrix}+\begin{bmatrix}\lambda_{n3} & \lambda_{n4}\end{bmatrix}\begin{bmatrix}C_{n3}e^{\lambda_{n3}x}\\ C_{n4}e^{\lambda_{n4}x}\end{bmatrix}\right\}\cos(k_n y). \tag{B.17}$$

where the complex C_{nr} terms are four unknown constants of integration. The λ_{nr} terms are determined by

$$\lambda_{n1,n2}=\pm\sqrt{k_n^2-k_L^2}\ \text{ and }\ \lambda_{n3,n4}=\pm\sqrt{k_n^2-k_T^2} \tag{B.18}$$

where $k_L^2=\rho\omega^2(1-\nu^2)/E$ and $k_T^2=2\rho\omega^2(1+\nu)/E$.

The first term of the integral in equation (B.15) can be rewritten as

$$\int_0^b\int_0^L\left|\frac{\partial u}{\partial x}\right|^2 dxdy=\int_0^b\int_0^L\left(\frac{\partial u}{\partial x}\right)\left(\frac{\partial u}{\partial x}\right)^* dxdy \tag{B.19}$$

where $$\frac{\partial u}{\partial x}=\sum_{n=1}^{n_{max}}\left\{\begin{bmatrix}\lambda_{n1} & \lambda_{n2}\end{bmatrix}\begin{bmatrix}C_{n1}\lambda_{n1}e^{\lambda_{n1}x}\\ C_{n2}\lambda_{n2}e^{\lambda_{n2}x}\end{bmatrix}+\begin{bmatrix}k_n & k_n\end{bmatrix}\begin{bmatrix}C_{n3}\lambda_{n3}e^{\lambda_{n3}x}\\ C_{n4}\lambda_{n4}e^{\lambda_{n4}x}\end{bmatrix}\right\}\sin(k_n y) \tag{B.20}$$

and $*$ denotes the complex conjugate.

Substituting equation (B.20) into equation (B.19),

$$\begin{aligned}
&\int_0^b\int_0^L\left[\left\{\sum_n\left(C_{n1}\lambda_{n1}^2e^{\lambda_{n1}x}+C_{n2}\lambda_{n2}^2e^{\lambda_{n2}x}+k_nC_{n3}\lambda_{n3}e^{\lambda_{n3}x}+k_nC_{n4}\lambda_{n4}e^{\lambda_{n4}x}\right)\right\}\right.\\
&\qquad\left.\left\{\sum_{n'}\left(C_{n'1}^*\lambda_{n1}^{*2}e^{\lambda_{n1}^*x}+C_{n'2}^*\lambda_{n2}^{*2}e^{\lambda_{n2}^*x}+k_{n'}C_{n'3}^*\lambda_{n3}^*e^{\lambda_{n3}^*x}+k_{n'}C_{n'4}^*\lambda_{n4}^*e^{\lambda_{n4}^*x}\right)\right\}\sin(k_n y)\sin(k_{n'}y)\right]dxdy\\
&=\frac{b}{2}\sum_n\left[|C_{n1}|^2|\lambda_{n1}|^4\frac{e^{2\mathrm{Re}(\lambda_{n1})L}-1}{2\mathrm{Re}(\lambda_{n1})}+|C_{n2}|^2|\lambda_{n2}|^4\frac{e^{2\mathrm{Re}(\lambda_{n2})L}-1}{2\mathrm{Re}(\lambda_{n2})}+\right.\\
&\qquad k_n^2|C_{n3}|^2|\lambda_{n3}|^4\frac{e^{2\mathrm{Re}(\lambda_{n3})L}-1}{2\mathrm{Re}(\lambda_{n3})}+k_n^2|C_{n4}|^2|\lambda_{n4}|^4\frac{e^{2\mathrm{Re}(\lambda_{n4})L}-1}{2\mathrm{Re}(\lambda_{n4})}+\\
&\qquad 2\mathrm{Re}\left\{C_{n1}C_{n'2}^*\lambda_{n1}^2\lambda_{n2}^{*2}\frac{e^{(\lambda_{n1}+\lambda_{n2}^*)L}-1}{\lambda_{n1}+\lambda_{n2}^*}+C_{n1}C_{n'3}^*\lambda_{n1}^2\lambda_{n3}^*k_n\frac{e^{(\lambda_{n1}+\lambda_{n3}^*)L}-1}{\lambda_{n1}+\lambda_{n3}^*}+\right.\\
&\qquad\qquad C_{n1}C_{n'4}^*\lambda_{n1}^2\lambda_{n4}^*k_n\frac{e^{(\lambda_{n1}+\lambda_{n4}^*)L}-1}{\lambda_{n1}+\lambda_{n4}^*}+C_{n2}C_{n'3}^*\lambda_{n2}^2\lambda_{n3}^*k_n\frac{e^{(\lambda_{n2}+\lambda_{n3}^*)L}-1}{\lambda_{n2}+\lambda_{n3}^*}+\\
&\qquad\qquad\left.\left.C_{n2}C_{n'4}^*\lambda_{n2}^2\lambda_{n4}^*k_n\frac{e^{(\lambda_{n2}+\lambda_{n4}^*)L}-1}{\lambda_{n2}+\lambda_{n4}^*}+C_{n3}C_{n'4}^*\lambda_{n3}\lambda_{n4}^*k_n^2\frac{e^{(\lambda_{n3}+\lambda_{n4}^*)L}-1}{\lambda_{n3}+\lambda_{n4}^*}\right\}\right]
\end{aligned} \tag{B.21}$$

where $\int_0^b \sin(k_n y)\sin(k_{n'} y)\,dy = \frac{b}{2}$ if $n = n'$.

The second term of the integral in equation (B.15) can be rewritten as

$$\int_0^b \int_0^L \left|\frac{\partial v}{\partial y}\right|^2 dxdy = \int_0^b \int_0^L \left(\frac{\partial v}{\partial y}\right)\left(\frac{\partial v}{\partial y}\right)^* dxdy \tag{B.22}$$

where $$\frac{\partial v}{\partial y} = -\sum_{n=1}^{n_{max}} k_n \left\{ \begin{bmatrix} k_n & k_n \end{bmatrix} \begin{bmatrix} C_{n1} e^{\lambda_{n1} x} \\ C_{n2} e^{\lambda_{n2} x} \end{bmatrix} + \begin{bmatrix} \lambda_{n3} & \lambda_{n4} \end{bmatrix} \begin{bmatrix} C_{n3} e^{\lambda_{n3} x} \\ C_{n4} e^{\lambda_{n4} x} \end{bmatrix} \right\} \sin(k_n y). \tag{B.23}$$

Substituting equation (B.23) into equation (B.22),

$$\begin{aligned}
&\int_0^b \int_0^L \left[k_n^2 \left\{ \sum_n \left(k_n C_{n1} e^{\lambda_{n1} x} + k_n C_{n2} e^{\lambda_{n2} x} + C_{n3} \lambda_{n3} e^{\lambda_{n3} x} + C_{n4} \lambda_{n4} e^{\lambda_{n4} x} \right) \right\} \right. \\
&\qquad \left. \left\{ \sum_{n'} \left(k_{n'} C_{n'1}^* e^{\lambda_{n1}^* x} + k_{n'} C_{n'2}^* e^{\lambda_{n2}^* x} + C_{n'3}^* \lambda_{n3}^* e^{\lambda_{n3}^* x} + C_{n'4}^* \lambda_{n4}^* e^{\lambda_{n4}^* x} \right) \right\} \sin(k_n y)\sin(k_{n'} y) \right] dxdy \\
&= \frac{b}{2} \sum_n k_n^2 \left[k_n^2 |C_{n1}|^2 \frac{e^{2\mathrm{Re}(\lambda_{n1})L} - 1}{2\mathrm{Re}(\lambda_{n1})} + k_n^2 |C_{n2}|^2 \frac{e^{2\mathrm{Re}(\lambda_{n2})L} - 1}{2\mathrm{Re}(\lambda_{n2})} + \right. \\
&\qquad |C_{n3}|^2 |\lambda_{n3}|^2 \frac{e^{2\mathrm{Re}(\lambda_{n3})L} - 1}{2\mathrm{Re}(\lambda_{n3})} + |C_{n4}|^2 |\lambda_{n4}|^2 \frac{e^{2\mathrm{Re}(\lambda_{n4})L} - 1}{2\mathrm{Re}(\lambda_{n4})} + \\
&\quad 2\mathrm{Re}\left\{ k_n^2 C_{n1} C_{n2}^* \frac{e^{(\lambda_{n1} + \lambda_{n2}^*)L} - 1}{\lambda_{n1} + \lambda_{n2}^*} + k_n C_{n1} C_{n3}^* \lambda_{n3}^* \frac{e^{(\lambda_{n1} + \lambda_{n3}^*)L} - 1}{\lambda_{n1} + \lambda_{n3}^*} + k_n C_{n1} C_{n4}^* \lambda_{n4}^* \frac{e^{(\lambda_{n1} + \lambda_{n4}^*)L} - 1}{\lambda_{n1} + \lambda_{n4}^*} + \right. \\
&\qquad \left. \left. k_n C_{n2} C_{n3}^* \lambda_{n3}^* \frac{e^{(\lambda_{n2} + \lambda_{n3}^*)L} - 1}{\lambda_{n2} + \lambda_{n3}^*} + k_n C_{n2} C_{n4}^* \lambda_{n4}^* \frac{e^{(\lambda_{n2} + \lambda_{n4}^*)L} - 1}{\lambda_{n2} + \lambda_{n4}^*} + C_{n3} C_{n4}^* \lambda_{n3} \lambda_{n4}^* \frac{e^{(\lambda_{n3} + \lambda_{n4}^*)L} - 1}{\lambda_{n3} + \lambda_{n4}^*} \right\} \right]
\end{aligned} \tag{B.24}$$

The third term of the integral in equation (B.15) can be rewritten as

$$2\nu \int_0^b \int_0^L \mathrm{Re}\left\{ \left(\frac{\partial u}{\partial x}\right)\left(\frac{\partial v}{\partial y}\right)^* \right\} dxdy. \tag{B.25}$$

Substituting equations (B.20) and (B.23) into equation (B.25),

$$2\nu\int_0^b\int_0^L\Bigg[\left\{\sum_n\left(C_{n1}\lambda_{n1}^2e^{\lambda_{n1}x}+C_{n2}\lambda_{n2}^2e^{\lambda_{n2}x}+k_nC_{n3}\lambda_{n3}e^{\lambda_{n3}x}+k_nC_{n4}\lambda_{n4}e^{\lambda_{n4}x}\right)\right\}$$

$$\left\{\sum_{n'}(-k_{n'})\left(k_{n'}C_{n'1}^*e^{\lambda_{n1}^*x}+k_{n'}C_{n'2}^*e^{\lambda_{n2}^*x}+C_{n'3}^*\lambda_{n3}^*e^{\lambda_{n3}^*x}+C_{n'4}^*\lambda_{n4}^*e^{\lambda_{n4}^*x}\right)\right\}\sin(k_ny)\sin(k_{n'}y)\Bigg]dxdy$$

$$=-\nu b\sum_n k_n\,\mathrm{Re}\Bigg[|C_{n1}|^2\lambda_{n1}^2k_n\frac{e^{2\mathrm{Re}(\lambda_{n1})L}-1}{2\mathrm{Re}(\lambda_{n1})}+|C_{n2}|^2\lambda_{n2}^2k_n\frac{e^{2\mathrm{Re}(\lambda_{n2})L}-1}{2\mathrm{Re}(\lambda_{n2})}+$$

$$|C_{n3}|^2|\lambda_{n3}|^2k_n\frac{e^{2\mathrm{Re}(\lambda_{n3})L}-1}{2\mathrm{Re}(\lambda_{n3})}+|C_{n4}|^2|\lambda_{n4}|^2k_n\frac{e^{2\mathrm{Re}(\lambda_{n4})L}-1}{2\mathrm{Re}(\lambda_{n4})}+$$

$$C_{n1}C_{n2}^*\lambda_{n1}^2k_n\frac{e^{(\lambda_{n1}+\lambda_{n2}^*)L}-1}{\lambda_{n1}+\lambda_{n2}^*}+C_{n1}C_{n3}^*\lambda_{n1}^2\lambda_{n3}^*\frac{e^{(\lambda_{n1}+\lambda_{n3}^*)L}-1}{\lambda_{n1}+\lambda_{n3}^*}+C_{n1}C_{n4}^*\lambda_{n1}^2\lambda_{n4}^*\frac{e^{(\lambda_{n1}+\lambda_{n4}^*)L}-1}{\lambda_{n1}+\lambda_{n4}^*}+$$

$$C_{n2}C_{n1}^*\lambda_{n2}^2k_n\frac{e^{(\lambda_{n2}+\lambda_{n1}^*)L}-1}{\lambda_{n2}+\lambda_{n1}^*}+C_{n2}C_{n3}^*\lambda_{n2}^2\lambda_{n3}^*\frac{e^{(\lambda_{n2}+\lambda_{n3}^*)L}-1}{\lambda_{n2}+\lambda_{n3}^*}+C_{n2}C_{n4}^*\lambda_{n2}^2\lambda_{n4}^*\frac{e^{(\lambda_{n2}+\lambda_{n4}^*)L}-1}{\lambda_{n2}+\lambda_{n4}^*}+$$

$$C_{n3}C_{n1}^*\lambda_{n3}k_n^2\frac{e^{(\lambda_{n3}+\lambda_{n1}^*)L}-1}{\lambda_{n3}+\lambda_{n1}^*}+C_{n3}C_{n2}^*\lambda_{n3}k_n^2\frac{e^{(\lambda_{n3}+\lambda_{n2}^*)L}-1}{\lambda_{n3}+\lambda_{n2}^*}+C_{n3}C_{n4}^*\lambda_{n3}k_n\frac{e^{(\lambda_{n3}+\lambda_{n4}^*)L}-1}{\lambda_{n3}+\lambda_{n4}^*}+$$

$$C_{n4}C_{n1}^*\lambda_{n4}k_n^2\frac{e^{(\lambda_{n4}+\lambda_{n1}^*)L}-1}{\lambda_{n4}+\lambda_{n1}^*}+C_{n4}C_{n2}^*\lambda_{n4}k_n^2\frac{e^{(\lambda_{n4}+\lambda_{n2}^*)L}-1}{\lambda_{n4}+\lambda_{n2}^*}+C_{n4}C_{n3}^*\lambda_{n4}\lambda_{n3}^*k_n\frac{e^{(\lambda_{n4}+\lambda_{n3}^*)L}-1}{\lambda_{n4}+\lambda_{n3}^*}\Bigg\}\Bigg] \qquad \text{(B.26)}$$

The last term of the integral in equation (B.15) can be rewritten as

$$\frac{(1-\nu)}{2}\int_0^b\int_0^L\left|\frac{\partial u}{\partial y}+\frac{\partial v}{\partial x}\right|^2dxdy=\frac{(1-\nu)}{2}\int_0^b\int_0^L\left(\frac{\partial u}{\partial y}+\frac{\partial v}{\partial x}\right)\left(\frac{\partial u}{\partial y}+\frac{\partial v}{\partial x}\right)^*dxdy \qquad \text{(B.27)}$$

where
$$\frac{\partial u}{\partial y}=\sum_{n=1}^{n_{\max}}k_n\left\{\begin{bmatrix}\lambda_{n1} & \lambda_{n1}\end{bmatrix}\begin{bmatrix}C_{n1}e^{\lambda_{n1}x}\\ C_{n2}e^{\lambda_{n2}x}\end{bmatrix}+\begin{bmatrix}k_n & k_n\end{bmatrix}\begin{bmatrix}C_{n3}e^{\lambda_{n3}x}\\ C_{n4}e^{\lambda_{n4}x}\end{bmatrix}\right\}\cos(k_ny) \qquad \text{(B.28)}$$

and

$$\frac{\partial v}{\partial x}=\sum_{n=1}^{n_{\max}}\left\{\begin{bmatrix}k_n\lambda_{n1} & k_n\lambda_{n2}\end{bmatrix}\begin{bmatrix}C_{n1}e^{\lambda_{n1}x}\\ C_{n2}e^{\lambda_{n2}x}\end{bmatrix}+\begin{bmatrix}\lambda_{n3}^2 & \lambda_{n4}^2\end{bmatrix}\begin{bmatrix}C_{n3}e^{\lambda_{n3}x}\\ C_{n4}e^{\lambda_{n4}x}\end{bmatrix}\right\}\cos(k_ny)\,. \qquad \text{(B.29)}$$

Substituting equations (B.28) and (B.29) into equation (B.27),

$$\frac{1-\nu}{2}\int_0^b\int_0^L\left[\left\{\sum_n\left(2k_nC_{n1}\lambda_{n1}e^{\lambda_{n1}x}+2k_nC_{n2}\lambda_{n2}e^{\lambda_{n2}x}+C_{n3}(k_n^2+\lambda_{n3}^2)e^{\lambda_{n3}x}+C_{n4}(k_n^2+\lambda_{n4}^2)e^{\lambda_{n4}x}\right)\right\}\right.$$

$$\left.\left\{\sum_{n'}\left(2k_{n'}C_{n'1}^*\lambda_{n1}^*e^{\lambda_{n1}^*x}+2k_{n'}C_{n'2}^*\lambda_{n2}^*e^{\lambda_{n2}^*x}+C_{n'3}^*(k_{n'}^2+\lambda_{n'3}^{*2})e^{\lambda_{n3}^*x}+C_{n'4}^*(k_{n'}^2+\lambda_{n'4}^{*2})e^{\lambda_{n4}^*x}\right)\right\}\cos(k_ny)\cos(k_{n'}y)\right]dxdy$$

$$=\frac{(1-\nu)b}{4}\sum_n\left[4k_n^2|C_{n1}|^2|\lambda_{n1}|^2\frac{e^{2\mathrm{Re}(\lambda_{n1})L}-1}{2\mathrm{Re}(\lambda_{n1})}+4k_n^2|C_{n2}|^2|\lambda_{n2}|^2\frac{e^{2\mathrm{Re}(\lambda_{n2})L}-1}{2\mathrm{Re}(\lambda_{n2})}+\right.$$

$$|C_{n3}|^2|k_n^2+\lambda_{n3}|^2\frac{e^{2\mathrm{Re}(\lambda_{n3})L}-1}{2\mathrm{Re}(\lambda_{n3})}+|C_{n4}|^2|k_n^2+\lambda_{n4}|^2\frac{e^{2\mathrm{Re}(\lambda_{n4})L}-1}{2\mathrm{Re}(\lambda_{n4})}+$$

$$2\mathrm{Re}\left\{4k_n^2C_{n1}C_{n2}^*\lambda_{n1}\lambda_{n2}^*\frac{e^{(\lambda_{n1}+\lambda_{n2}^*)L}-1}{\lambda_{n1}+\lambda_{n2}^*}+2k_nC_{n1}C_{n3}^*\lambda_{n1}(k_n^2+\lambda_{n3}^{*2})\frac{e^{(\lambda_{n1}+\lambda_{n3}^*)L}-1}{\lambda_{n1}+\lambda_{n3}^*}+\right.$$

$$2k_nC_{n1}C_{n4}^*\lambda_{n1}(k_n^2+\lambda_{n4}^{*2})\frac{e^{(\lambda_{n1}+\lambda_{n4}^*)L}-1}{\lambda_{n1}+\lambda_{n4}^*}+2k_nC_{n2}C_{n3}^*\lambda_{n2}(k_n^2+\lambda_{n3}^{*2})\frac{e^{(\lambda_{n2}+\lambda_{n3}^*)L}-1}{\lambda_{n2}+\lambda_{n3}^*}+$$

$$\left.\left.2k_nC_{n2}C_{n4}^*\lambda_{n2}(k_n^2+\lambda_{n4}^{*2})\frac{e^{(\lambda_{n2}+\lambda_{n4}^*)L}-1}{\lambda_{n2}+\lambda_{n4}^*}+C_{n3}C_{n4}^*(k_n^2+\lambda_{n3}^2)(k_n^2+\lambda_{n4}^{*2})\frac{e^{(\lambda_{n3}+\lambda_{n4}^*)L}-1}{\lambda_{n3}+\lambda_{n4}^*}\right\}\right] \qquad \text{(B.30)}$$

The strain energy for in-plane vibration can be analytically obtained from equations (B.21), (B.24), (B.26) and (B.30).